On the simulation of northeast monsoon rainfall over southern peninsular India in CMIP5 models

sreekala pp (sreekalacusat@gmail.com)
Cochin University of Science and Technology
C.A. Babu
Cochin University of Science and Technology
S.VijayaBhaskara Rao
Cochin University of Science and Technology

Research Article

Keywords: CMIP5, NEMR, El Nino, PIOD

Posted Date: February 23rd, 2021

DOI: https://doi.org/10.21203/rs.3.rs-248048/v1

Abstract

The skill of 34 CMIP5 models to simulate the mean state and interannual variability of Northeast Monsoon Rainfall (NEMR) is studied here. The mean (1979–2005) NEMR over southern Peninsular India (SPIRF), Indian Ocean and Maritime continents (10°S-30°N,40°E-120°E) is simulated reasonably well by CMIP5 models with pattern correlation ranges from 0.6 to 0.93. A few individual models have been found to be outperformed the multi model ensemble (PCC-0.88). Diverse behaviour in the simulation of Indian and Pacific Ocean SST is observed in the CMIP5 models. A set of models (high skill models: HSM), which shows an NIOD like mean (1979–2005) SST bias in Indian Ocean and strong La Nina like mean SST bias in the Pacific Ocean, are able to simulate the mean NEMR more realistically. Another set of models (low skill models: LSM) which shows a Positive IOD (PIOD) like mean SST bias in the Indian Ocean and a weak La Nina like mean SST bias in the Pacific Ocean are not able to simulate the observed equatorial Indian Ocean westerlies. This leads to an abnormal ascending motion and unrealistic wet bias over the western Indian Ocean and dry bias over the southern Peninsular India, southeast Asia and southeast Indian Ocean. Observational analysis reveals that the ascending anomalies over warm pool in the climatological mean Walker circulation during NEM season is modified as ascending anomalies to the east and west of warm pool region and descending anomalies over warm pool region during El Nino and PIOD. This modulation is manifested as an interesting pattern of warm and wet western Indian Ocean, southern Peninsular India and central and eastern Pacific Ocean and cool and dry warm pool region including Maritime continents.The observation analysis also reveals that the establishment of South China Sea anticyclone and Bay of Bengal anticyclone during El Nino and PIOD are strongly related with the ascending motion over south peninsular India and hence enhances the south Peninsular Indian rainfall during NEM season. Around 70% of the CMIP5 models were not able to capture the observed positive correlation that exist between SPIRF and Nino3.4 SST as well as SPIRF and DMI. An unrealistic westward extension of warm anomalies over the equatorial Pacific cold tongue is observed in low skill models (LSM-IAV). Unrealistic westward extension of South China Sea anticyclone and Bay of Bengal anticyclone (up to 70°E) is also observed in the LSM-IAV model ensemble. This is manifested as the abnormal descending anomalies and unrealistic dry bias over the southern Peninsular India and hence the unrealistic negative CC between SPIRF and Nino 3.4 SST (SPIRF-DMI). The descending anomalies over South China Sea and ascending anomalies over the western Indian Ocean and southern Peninsular India (50°E-80°E) is well captured but with lower intensity in HSM-IAV and hence it shows the observed positive CC between SPIRF and Nino3.4 SST as well as SPIRF and DMI.

1. Introduction

Indian subcontinent experiences two monsoons, the southwest or summer monsoon (June to September) and the northeast or winter monsoon (October-December). While the summer monsoon is responsible for 80% of the total rainfall of the country (Gadgil 2006; Parthasarathy et al. 1994), the northeast monsoon rainfall is also important especially for its southern states. Northeast (NE) monsoon is a part of the northeast trades and is dry, stable, and has less vertical extent compared to southwest monsoon (Dhar

and Rakhecha, 1983). During the onset phase of northeast monsoon (October third week) low level wind over India reverses its direction from southwesterlies to northeasterlies. This change is associated with the southward movement of continental tropical convergence zone (CTCZ) and the sub-tropical anticyclone. With this southward movement of CTCZ, a trough gets established over the south Bay of Bengal. Southern peninsular India receives ample amount of rainfall mainly from the low-pressure systems that form in the trough.

The region of southern peninsula demarcated by the Indian Peninsula south of 15°N proposed by Singh and Sontakke (1996) is more appropriate for the study of northeast monsoon rainfall variability. This region consists of six subdivisions of India Meteorological Department viz., Coastal Andhra Pradesh, Rayalaseema, South Interior Karnataka, Coastal Karnataka, Tamil Nadu, and Kerala. These subdivisions receive 17–49% of their annual rainfall while the country as a whole receives only 11% of its annual rainfall (Sreekala et al. 2012). Northeast monsoon rainfall (NEMR) shows high temporal variability with a coefficient of variation 25% compared to southwest monsoon (10%) (Nageswara Rao 1999; Rajeevan et al. 2012). Since most of the subdivisions of southern peninsular Indiaare under rain shadow region during the summer monsoon season, the agricultural production of these subdivisions is largely determined by the interannual variability of NEMR over southern peninsular India. A significant drop in agricultural production is noticed during deficient NEMR years. (Kumar et al. 2007; Rao and Jaganathan 1953).

The previous studies reveal that the interannual variability of NEMR is related to the El Nino Southern Oscillation (ENSO) and Indian Ocean Dipole (IOD) in such a way that the positive (negative) phase of ENSO and IOD enhances (suppresses) the rainfall over thesouthern peninsular India during NEM season (Bhanu Kumar et al. 2004; Kripalani and Kumar 2004; Suppiah 1996, 1997; De and Mukhopadhyay 1999; Kumar et al. 2007; Rajeevan et al. 2012; Yadav 2012; Sreekala et al. 2012; Sreekala et al. 2018).The above normal SST over the central and eastern Pacific Ocean and western Indian Ocean and below normal SST over the western Pacific Ocean and south eastern Indian Ocean is related to the El Nino and Positive phase of IOD (PIOD) and a similar SST anomaly pattern is observed during excess NEMR years (Sreekala et al. 2012, Sreekala et al. 2018, Yadav 2012). During the positive phase of ENSO and IOD, the anomalous flow pattern shows winds converging and moisture transport from the south eastern Indian Ocean and the Bay of Bengal towards southern peninsular India (Sreekala et al. 2012, Kripalani and Kumar 2004, Rajeevan et al. 2012). Recent study by Sreekala et al. 2018 revealed that a similar mode of physical mechanism is responsible for the intraseasonal and interannual variability of northeast monsoon rainfall and anomalous rainfall (positive rainfall anomalies over southern peninsular India and western Indian Ocean) outgoing long wave radiation (negative OLR anomalies over southern peninsular India, positive OLR over east Indian and western Pacific Ocean), SST (positive SST anomalies over Central Pacific Ocean), and 850 hPa wind (easterly wind anomaly over Equatorial Indian Ocean) pattern is similar to the positive phase of ENSO and IOD and the first three phases of MJO.

Thereisa secular variationexists in the relationship of NEMR and ENSO (Zubair and Ropelewski 2006; Kumar et al. 2007; Rajeevan et al. 2012; Yadav 2012; Yadav 2013). The ENSO-NEMR relationship has

strengthened during 1980s and 1990s (Zubair and Ropelewski 2006; Kumar et al. 2007; Yadav 2012) and weakened during 2010s (Rajeevan et al. 2012; Yadav 2013). Recent study by Yadav, 2013 revealed that the east–west asymmetry in the warming of the tropical Indian Ocean by ENSO and IOD after the 1976/77 climate shift was favourable to NEMR but the relationship has weakened during the recent decade 2001-2011 and a north-south asymmetry in the warming of the tropical Eastern Indian Oceanwhich is also present during El Nino and PIOD remains favourable in the recent decade 2001-2011. He proposed a new index GSST, gradient of SST between East Bay of Bengal (88.5°E–98.5°E; 8.5°N–15.5°N) and EEIO boxes (80.5°E–103.5°E; 6.5°S–3.5°N), which has high correlation with NEMR in such a way that the excess(deficient) NEMR years are found to be during the positive (negative) GSST years.

The climate model studies based on carefully constructed scenarios of emission of greenhouse gases arehelpful to understand the effect of global warming on the northeast monsoon. The modelling studies on the northeastmonsoon is very limited. Raj et al. (1993, 2004) and Raj (1998) have explored the skill of predicting theinterannual variability of the NEMR using statistical methods and the models show a very poor prediction skill. Dynamical modelling studies of NEMR are also very limited (Acharya et al. 2011; Archana et al. 2013; Rajeevan et al. 2012). A poor skill in simulating the mean state and interannual variability of northeast monsoon by coupled models is noticed in recent studies (Rodwell 2005; Rajeevan et al. 2012; Siew et al. 2014). The hindcast analysis for the period 1960-2005 by Rajeevan et al (2012) reveals the inability of ENSEMBLE models to simulate the observed positive correlation between the El Nino and NEMR properly.

As a part of the preparation of Intergovernmental Panel on Climate Change (IPCC)Fifth Assessment Report (AR5), the Coupled Model Inter comparison Project phase5 (CMIP5) has been conducted and a number of international climate science research groups performed a broad set of climate runs (Taylor et al., 2012). IPCC-CMIP5 models provide substantial experiment outputs which can be used for studying the climate variability. Many studies areavailable on the summer monsoon rainfall variability and its future projection in CMIP5 models (Sabeer et al. 2015; Bin Wang et al. 2015; Menon et al. 2013; Ramuet al. 2017; Roy et al. 2018; Ramuet al. 2019). Recently Prasanna et al. (2019) has studied the multiyear La Nina events and its relation with NEMR by using observations and 20 CMIP5 models. Prasanna et al. (2020) has also studied the diversity in ENSO remote connection to northeast monsoon rainfall in the observations and 11 CMIP5 models. Both these studies explained the poor skill of CMIP5 models in simulating the NEMR-ENSO teleconnection.

So far there are no studies available which explains the skill of CMIP5 models to simulate the mean state of NEMR. The present study is meant to give a proper picture about the skill of 34 CMIP5 models in simulating the mean state and interannual variability of northeast monsoon rainfall over southern peninsular India (SPIRF). The interannual variability of NEMR in relation with El Nino and PIOD in CMIP5 models are extensively studied here.Here we analysed the El Nino and PIOD related SST, rainfall and circulation anomalies over Indian and Pacific Ocean. East-west and north-south asymmetry in the warming of tropical Indian Ocean during El Nino and PIOD influences the northeast monsoon rainfall over the southern peninsular India (Yadav, 2013). East-west asymmetry in SST causes changes in the Walker

circulation while north-south asymmetry causes changes in the Hadley circulation. Here, we analysed the modulation of Walker and Hadley circulation by El Nino and PIOD in the actual observation and in the CMIP5 models. These analyses will help to explain the reasons behind the poor skill in simulating theEl Nino-NEMR and PIOD-NEMR direct relationship in the models

2. Data And Methodology

Thehistorical simulations (1850-2005) from the Fifth Coupled Model Inter-comparison (CMIP5) are used here for the analysis. We analysed the monthly datasets of 34 CMIP5 model output (one ensemble member: r1i1p1) for a common period 1979-2005. The details of 34 models are given in the Table 1. The monthly SST from the Hadley Centre Sea Ice and SST datasets (HadISST) is used for calculating the Nino3.4 SST index and dipole mode index and spatial regression analysis. Since there exists a simultaneous correlation between SPIRF and Nino 3.4 as well as SPIRF and DMI (De andMukhopadhay1999; Bhanu Kumar et al.2004; Kripalani and Kumar2004; Zubair and Ropelewski2006; Kumar et al.2007; Sreekala et al.2012, Yadav2012, Zubair et al.2003), we calculated three month (Oct-Dec) mean of SST over Nino 3.4 region (5°S–5°N, 170°W–120°W) and three month mean of dipole mode index [DMI : difference in SST between the tropical western Indian Ocean (50°E–70°E, 10°S–10°N)and the south eastern Indian Ocean (90°E–110°E, 10°S-Equator)]by using HadISST and model SST datasets.

The monthly datasets of zonal, meridional and vertical wind (multilevel) from European Centre for Medium-Range Weather Forecasts (ECMWF) ERA-5 reanalysisare used to study the large-scale circulation features and Hadley and Walker circulation associated with El Nino and PIOD. The GPCP (Global Precipitation climatology Project) datasets (Huffman et al.1997; Adler et al.2003) is used for the rainfall analysis which is available from 1979 onwards. GPCP datasets are useful for various climatological applications and is prepared by merging the low-orbit satellite microwave data, geosynchronous-orbit infrared data, and surface rain gauge observations over land using the inverse variance weighting method (Xie et al. 2003; Shin et al.2011). The simultaneous correlation coefficient (CC) between NEMR series and gridded precipitation data (GPCP) for the period1982–2010 over southern peninsular India is 0.85, which suggests the consistency and accuracy among the datasets (Yadav 2013).The observational and model datasets of rainfall, SST, zonal, meridional and vertical wind (at various levels) are interpolated into a common 2°x2° degree horizontal grid resolution and all the three wind components are interpolated into a common 13 vertical grid resolution (1000, 925, 850, 800, 700, 600, 500, 400, 300, 200, 150, 100hPa).

For model evaluation, different techniques such as Taylor diagram, difference of mean climatology, spatial regression etc. were used. Taylor diagram provides the pattern correlation and normalised variance, which provides comprehensive summary statistics of the model performance (Taylor 2001). To evaluate the skill of CMIP5 models in simulating the mean state of northeast monsoon, we categorised the CMIP5 models intohigh skill and low skill models based on the pattern correlation and root mean square error. The ensemble of five high skill models (HSM) and five low skill models (LSM) are compared with the observation. Similarly, based on the correlation coefficient between the SPIRF and Nino3.4 SST

as well as SPIRF and DMI, five high skill models' ensemble (HSM-IAV) and low skill models'ensemble (LSM-IAV) were analysed to explore the skill of models to capture the interannual variability of SPIRF in association with El Nino and PIOD.

The spatial regression maps of Nino 3.4 SST (and DMI) onto rainfall, SST and 850hPa wind for observation and models have been made for further analysis. The mean (1979-2005) Walker (Hadley) cell circulation are obtained by averaging the zonal (meridional) and pressure vertical velocity between 5°S and 5°N (60°E and 85°E) by using ERA5 datasets and CMIP5 model output datasets.

To study the modulation of Walker (Hadley) circulation by El Nino and PIOD, zonal(meridional) and vertical wind are averaged between 5°S and 5°N (60°E and 85°E) and then calculated the regression of Nino 3.4 SST as well as DMI on to the zonal (meridional) and vertical wind and the structure of Walker (Hadley) circulation obtained by the regressed zonal (meridional) and vertical winds. The Walker circulation over Northern latitudes (5°N-15°N) also studied for the further understanding.

3. Mean State Of Northeast Monsoon In Cmip5 Models

The fidelity of CMIP5 models in simulating the mean climatology of northeast monsoon rainfall is discussed in this section. Global Precipitation Climatology Project (GPCP) rainfall data (Adler et al. 2003) from 1979 to 2005 has been used for the comparison of mean seasonal (Oct-Dec) simulated and observed rainfall pattern. The model performance in simulating the spatial pattern of NEMR over South Peninsular India and Indian Ocean region (10°S-30°N,40°E-120°E) is given by the Taylor diagram. The pattern correlation coefficient (PCC) and normalised standard deviation of different models and multi model ensemble (MME) in the Taylor diagram indicate that the PCC of different models is in the range of 0.6 and 0.93 while the PCC of MME is 0.88. Normalised standard deviation is in between 1 to 1.8 for the models (Fig.1). Pattern correlation of CMIP5 models for southwest monsoon season is below 0.8 for most of the models and the multi model ensemble (MME) is closer to the observations than any of the individual models (Rajiv et al. 2012). But in the case of NEMR, there are a few models which outperformed the MME. The ratio of PCC to RMSE (Root mean square error) in the CMIP5 models gives a good measure for its skill (Table 2). The ratio of a few models is higher (0.47-0.69) than that of the MME (0.46). So, here we considered five models (MPI_LR, MPI_MR, GFDLESM2G, GFDLCM2.1and CanESM2) which have high ratio (more than 0.54) as high skill models and five models (MRI_CGCM3, ACCESS1-3, CMCC_CMS, HadGEM2-ES and HadGEM2-CC) which have ratio less than 0.2 as low skill models. The ensembles of high skill models (HSM) and low skill models (LSM) are considered for the comparison of simulated and observed northeast monsoon rainfall.

During NEM season, maximum rainfall zone is observed over the south eastern Indian Ocean and it decreases substantially to the western direction and minimum rainfall is observed over the western Indian Ocean (Fig. 2). Over land, the southeastern peninsular India receives maximum rainfall and it decreases towards northwest direction. The bias in the mean (1979-2005) rainfall (mm/day) of HSM, LSM and MME is analysed and compared here (Fig.2). Positive bias in rainfall over the southwestern Indian Ocean

and negative bias in rainfall over the southeastern Indian Ocean, the southern Bay of Bengal and the southeast India is observed in all the three ensembles (MME, HSM and LSM) with varying intensities. A maximum bias in the rainfall of more than 7mm/day (less than 4mm) is observed over thesouthwestern Indian Ocean and -5 mm/day (-2mm) is observed over the southeastern Indian Ocean in LSM (HSM). Thus, a westward extension of maximum zone of NEMR over the Indian Oceanis a major error found in the models. The possible reason behind the unrealistic simulation of rainfall can be revealed by comparing the spatial pattern of mean sea surface temperature (SST) and wind circulation in the models to the observations.

In tropics, the mean column water vapour (CWV) controls the precipitation (Raymond 2000; Bretherton et al. 2004). The sources for CWV includes low level moisture convergence, surface evaporation, moisture convection and cloud radiation feed backs (Bretherton et al. 2004). A necessary condition for the abundance of CWV over moist convective regions is high mean SST of more than 28°C (Neelin et al. 2009). So, the misrepresentation of SST in the models can lead to the precipitation errors. The mean SST bias in HSM, LSM and MME is compared here. In LSM and MME, a positive SST bias of 0.2-0.4°C is noticed over the south western Indian Ocean where we find a large erroneous positive bias in the precipitation (Fig.3). The absence of such positive SST bias over southwestern Indian Ocean in HSM may lead to the realistic simulation of NEM rainfall. Previous study by Ibnu Fathrio et al. (2017) suggest that the SST bias over the southwestern Indian Ocean is induced by biases in the East African Coastal current and South Equatorial Counter Current which is associated with biases of thermocline depth in the southwestern Indian Ocean. Thus, it implies that the correct simulation of Ocean-Atmospheric interactionis necessary for a realistic simulation of SST over Indian Ocean.

The positive (negative) SST bias over the south eastern Indian Ocean in HSM (LSM) is similar to the SST anomaly during PIOD (Negative phase of IOD). Excessive cold tongue SST bias is a well-known error in CMIP5 models and considered as an important source of bias in the projections of ENSO under global warming (Li and Xie 2012; Zheng et al. 2012; Li et al. 2015). Here, we find that this error is more pronounced in HSM rather than in LSM and MME. Along with the cold tongue error, a strong warm bias over the western Pacific and the north eastern Pacific in HSM and a positive bias in SST over the northern and southern part of equatorial cold tongue in LSM are noticed. Overall, negative IOD and strong La Nina like bias in the mean state of SST is observed in HSM while Positive IOD and weak La Nina like bias in the mean state of SST is observed in LSM. Previous studies suggested that positive (negative) phase of ENSO and IOD enhances rainfall over western Indian Ocean (Sreekala et al. 2018; Yadav 2013). Obviously positive IOD like mean state SST bias in LSM could lead to the excess rainfall bias over Western Indian Ocean. But negative IOD and La Nina like mean SST bias in HSM could not explain the wet bias in precipitation over the southwestern Indian Ocean in HSM. And how these SST biases lead to a smaller dry biasof SPIRF in HSM than in LSM also could not explain merely by La Nina, NIOD and PIOD like mean states in HSM and LSM respectively. Hence, we analysed the zonal, meridional and vertical circulations in the LSM and HSM in detail to understand the reasons behind diversity in the precipitation biases in CMIP5 models.

Mean 850hPa wind pattern simulated by HSM and LSM is compared with the observation for the further analysis. Generally, atmospheric convection over the eastern equatorial Indian Ocean and Maritime continent is strong and hence trade winds are absent in the equatorial Indian Ocean (Gill, 1980). Semi-annual westerly winds over the equatorial Indian Ocean are observed in the intermonsoon season. October to December period is such an intermonsoon season with strong westerlies over the equatorial Indian Ocean. Here,in the observation,we found that the prevailing wind is north easterlies which blows over the northwestern Pacific Ocean, Bay of Bengal and Arabian Sea. The north easterlies over Arabian Sea recurve at around 5°N latitude and blows as equatorial westerlies over the equatorial Indian Ocean (Fig.4). This observed circulation pattern is reasonably well captured but with lower intensity and erroneous eastward shift up to 120°E in HSM (Fig.4). The observed equatorial westerlies are absent in LSM. In LSM, instead of recurving at 5°N, the north easterlies from the Arabian Sea blows towards the southwestern Indian Oceanand converge with south easterlies from the south Indian Ocean and causes for a strong wet bias over the south western Indian Ocean.

Mean wind bias for HSM and LSM shows a strong easterly bias (5-6m/s) over the Indian Ocean in LSM while a very weak bias in the easterly wind over the Indian Ocean in HSM (Fig.3). A strong easterly wind bias over the western Pacific is observed in HSM. Easterly wind bias in LSM and HSM are consistent with the east-west gradient in the SST bias in Indian and Pacific Ocean respectively. Wyrtki jets which is developed as a direct response of equatorial westerlies carry mass and heat from the western Indian Ocean to the eastern equatorial Indian Ocean and helps to deepen the thermocline in the eastern equatorial Indian Ocean (O'Brien and Hurlburt1974; Schott and McCreary2001; Rao and Sivakumar2000). The absence of equatorial westerlies and presence of strong easterly wind bias in LSM may inhibit the development of Wyrtki jets and altered the actual Bjerknes feedback present over Indian Ocean. Thus, as we explained earlier PIOD like unrealistic warm western Indian Ocean, cool eastern Indian Ocean and the presence of strong easterlies over the equatorial Indian Ocean in LSM are responsible for the strong wet bias over the southwestern Indian Ocean.

The mean (1979-2005) Hadley and Walker circulation during NEM season in HSM, LSM is compared with the observation to understand the reasons behind the dry bias in SPIRF in LSM. The structure of the Hadley (Walker) circulation is obtained by averaging the zonal (meridional) and vertical velocity between 60°E and 80°E (5°N and 5°S). Previous studies propose that the meridional distribution of tropical SST influence the spatial variation of Hadley Circulation (Li and Fing 2017) by altering the strength and position of convergence (Shneider and Lindzen1977) and vertical motion (Lindzen and Nigam 1987). A strong cold SST bias over the northern Arabian Sea and northern Bay of Bengal and a strong warm SST bias over the westernequatorial Indian Oceanleads to a strong gradient in SST from the equator to the northern latitudes in LSM. This is manifested as an unrealistic strong bias in ascending motion and hence a strong wet bias over equatorial western Indian Ocean (5°S-5°N,60°E-80°E) in LSM (Fig.5). Descending bias over the southern Peninsular India (10°N-15°N) is observed in LSM which leads to a dry bias in precipitation over there. Compared to LSM, north-south gradient in SST over the equatorial western Indian Ocean is weaker in HSM and hence the ascending and descending biases are also weaker in HSM and hence HSM ensemble shows a better simulation of precipitation over the western Indian

Ocean and southern peninsular India. This explains the changes in the simulation of north-south SST gradient in the models are responsible for the observed dry bias in SPIRF in CMIP5 models.

While the north-south asymmetry in SST in the models leads to the changes in Hadley circulation, the east-west asymmetry in SST in the models makes changes in the Walker circulation. The east-west SST bias in the Indian Ocean (cool eastern and warm western Indian Ocean) and the Indo-Pacific Ocean (warm SST over eastern Indian and western Pacific Ocean and cool SST over central and eastern Pacific Ocean) is responsible for the strong biases in the Walker circulation in LSM and HSM respectively (Fig. 6). Consistent with east-west asymmetry in SST biases, strong unrealistic ascending motion is present over the western Indian Ocean in LSM which is responsible for the western Indian Ocean precipitation bias, while this type of ascending motion is weaker in HSM which leads to a better simulation of precipitation over there. Due to the La Nina like SST biases in both the ensembles, an unrealistic descending motion is present over the central and eastern Pacific Ocean and ascending motion over the equatorial eastern Indian and the western Pacific Ocean which is more intense in HSM rather than in LSM.

4. Interannual Variability Of Northeast Monsoon Rainfall Variability Over Southern Peninsular India

The interannual variability in NEMR over the southern peninsular India (SPIRF) is very high with a coefficient of variation of 26.11% (Sreekala et al. 2012). Previous studies indicate that the interannual variability of NEMR is primarily controlled by the ocean–atmosphere phenomena like El Nino Southern Oscillation (ENSO) and Indian Ocean Dipole. The positive phase ofENSO and IOD generally favours the NEMR over southern peninsular India (Kumar et al. 2007; De and Mukhopadhay 1999; Zubair and Ropelewski 2006; Yadav 2012; Sreekala et al. 2012; Kripalani et al. 2004; Kumar et al. 2007). In this section, the skill of CMIP5 models in simulating this direct relationship between ENSO (IOD) and NEMR is analysed. A significant simultaneous positive (OND period) correlation exists between SPIRF and Nino 3.4 SST as well as SPIRF and Dipole mode index (Sreekala et al. 2012). The correlation coefficient of the SPIRF with Nino3.4 SST and DMI for a period 1979-2005 for 34 CMIP5 models are given in the Table 3. Around 70% of the selected models were not able to reproduce the observed positive correlationbetween El Nino and SPIRF as well as PIOD-SPIRF. Previous analysis of seasonal hindcast (1996-2005) produced by the state-of-the-art coupled climate model ENSEMBLES also revealed that the coupled models have very poor skill in predicting the interannual variability of the NEMR (Rajeevan et al. 2012) due to the inability of the ENSEMBLES models to simulate the positive relationship between ENSO and the NEMR correctly. Here also, we get a similar result for most of the models which shows a strong negative correlation coefficient between the Nino 3.4 SST and SPIRF as well as DMI and SPIRF. We did an in-depth analysis to understand why the models have poor skill in simulating theEl Nino-SPIRF and PIOD-SPIRF direct relationship.

Generally, we found that the models which shows positive correlation between Nino3.4 SST and SPIRF also shows a positive correlation betweenDMI and SPIRF. Surprisingly we also noticedthat the models in

HSM category in mean state simulation except MPI_MR and CMCCCESM are not able to capture the positive correlation between Nino3.4 SST-SPIRF and DMI-SPIRF. Similarly, the models in LSM category in mean state simulation were able to capture the observed positive correlation between Nino3.4 SST-SPIRF and DMI-SPIRF. So, here we selected six models (BCC-CSM1.1, CMCC-CESM, IPSL-CM5A-LR, MPI-ESM-MR, MRI-CGCM3) which have positive CC between Nino3.4 SST and SPIRF and also between DMI and SPIRF. An ensemble of these six models (HSM-IAV) is used for further analysis. We have selected another six models (CanESM2, CCSM4, GFDL-CM3, GFDL-ESM2M, GFDL-ESM2G) which have better pattern correlation and RMSE for mean rainfall simulation but negative CC between Nino3.4SST and SPIRF (DMI-SPIRF). These models are considered as low skill models for interannual variability simulation. An ensemble of these six models (hereafter, LSM-IAV) is used for further analysis.

Spatial regression maps of Nino 3.4 SST onto the rainfall, SST and surface wind of the HSM-IAV and LSM-IAV are made and compared with the spatial regression maps of Nino3.4 SST (HadISST) onto the observed rainfall (GPCP), SST (HadISST) and surface wind (ERA5). This section is divided into two subsections: one for observation and other for CMIP5 models.

4.1 Observed SST-wind-rainfall anomalies associated with El Nino and PIOD

The SST (HadISST), wind (ERA5) and rainfall (GPCP) relationship as per Bjerknes feedback is depicted clearly in the spatial regression maps (Fig.7c). Over Indian Ocean, El Nino is associated with the anomalous positive SST over the western Indian Ocean, north equatorial Indian Ocean and anomalous negative SST over the south eastern Indian Ocean. Here, we note that the SST and rainfall anomalies are roughly collocated over the Indian Ocean. In accordance with the SST pattern, anomalous south easterlies are blowing to the north of the equator (hence towards southern peninsular India) and anomalous north easterlies are blowing to the south of the equator. The east-west SST gradient in the equatorial Indian Ocean (EIO) is responsible for the zonal component of wind anomalies in EIO (easterlies) while the north-south SST gradient such as below normal SST over the southernequatorial Indian Ocean (0-20°S) and above normal SST over North Indian Ocean is responsible for the meridional component of wind anomalies (southerlies). An anomalous anticyclonic circulation over the Bay of Bengal is observed in the wind regression pattern. This anticyclone is forced by the reduction of deep convection over the Maritime continent which is related to El Nino (Sengupta et al, 2019). Due to this anticyclonic circulation, the number of tropical cyclones forms over Bay of Bengal is below (above) normal during El Nino year (La Nina year) (Girshkumar et al.2015). Even though the number of cyclones forms over Bay of Bengal is less during El Nino, these cyclones often strike the southern peninsular India.The number of cyclones over Bay of Bengal is more during La Nina but these cyclones recurve and move towardsnorth western direction and miss the southern Peninsular India(Yadav, 2013;Girshkumaret al. 2015; Sreekala et al. 2018).The anomalous circulation over the Indian Ocean is important in bringing moisture towards the southern peninsular India and hence make an El Nino year to be an above normal NEMR year as proposed by a few previous studies (Kumar et al.2007;Yadav et al.2012;Sreekala et al.2012). Above normal rainfall over the western Indian Ocean and below normal rainfall over eastern Indian Ocean and maritime continents is also associated with the positive phase of ENSO.

Over Pacific Ocean, anomalous positive SST over the equatorial central Pacific and anomalous negative SST over the western Pacific and northern and southern central Pacific Ocean is related to the El Nino. Strong westerlies are observed over cold tongue region. An anticyclonic circulation exists over South China Sea. These anomalous SST and wind circulation patterns lead to the excess rainfall over the equatorial central Pacific while deficient rainfall over the southeast Asia, western Pacific and northern and southern part of central Pacific Ocean during El Nino.In this study, we are trying to understand how El Nino leads to the excess rainfall anomalies over southern Peninsular India in observation as well as in CMIP5 models. SPIRF is found to be positively correlated with the north western Pacific Sea level pressure and divergence anomalies (Yadav 2012; Sreekala et al. 2012). Here we find an anticyclonic circulationover south China Sea. This anomalous anticyclone is generated via the atmospheric Rossby wave response to the convective cooling anomalies around the western tropical Pacific which is associated with ENSO (Zhang et al. 1996; Wang et al. 2000; Feng et al. 2010). This anticyclone is rapidly developed around mid-October and is related to the reversal of vertical motion over Indian Ocean from downward to upward and it is found to be controlled by south western Indian Ocean SST anomalies (Watanabe et al.2002; Annamalai et al. 2005; Du et al. 2009). So, it will be interesting to check how El Nino modulates the Hadley and Walker circulation over the Indian Ocean and its linkage with the SPIRF. Third section of this study explores the modulation of Hadley and Walker cell circulation by El Nino and PIOD in detail.

Indian Ocean Dipole is the major mode of Indian Ocean coupled system which can either be internally forced or externally generated by ENSO (Schott et al. 2009). In this study we understand that during the NEM season, both Nino 3.4 SST and DMI is associated with a similar pattern of SST, wind and rainfall anomalies over Pacific and Indian Ocean (Fig. 8c). Both ENSO and IOD is developing through positive Bjerknes feedback where zonal SST gradient and zonal wind stress plays an important role. ENSO and IOD is linked through Walker circulation and generally El Nino (La Nina) and Positive IOD (Negative IOD) are co-occurring in Pacific and Indian Ocean respectively (Mayers et al. 2007; Santaso et al. 2017). Similarity in the mechanism behind the formation of ENSO and IOD and its interconnection explains the similarity in the anomalous SST, wind and rainfall pattern during El Nino and PIOD (Fig. 6). Compared to El Nino, more intense anomalies are associated with PIOD. Even though a few dissimilarities are also observed in theEl Nino and PIOD regression maps. One such dissimilarity is the PIOD related positive rainfall anomalies over the north western Indian Ocean (10°N-25°N) and adjoining land areas including north Indian land. Compared to El Nino, westward extension of both cold tongue and south eastern Indian Ocean cold SST anomaliesis less during PIOD (Figs. 7c and 8c).

4.2 SST-wind-rainfall anomalies associated with El Nino and PIOD in CMIP5 models

The anomalous SST, wind and rainfall patterns related to the positive phase of ENSO in the model ensembles (HSM-IAV) and (LSM IAV) and its differences are shown in the Figure 9. Above normal SST anomalies over the western Indian Ocean and below normal SST anomalies over the south eastern Indian Ocean associated with El Nino is better simulated not by HSM-IAV but by LSM-IAV. An unrealistic cold bias over equatorial east and central Indian Ocean and warm bias over south eastern Indian Ocean is

present in HSM-IAV. Similar to the observation, the zonal wind anomalies over Indian Ocean are easterlies in both HSM-IAV and LSM-IAV. But these equatorial wind anomalies also have a meridional component (southerly wind) which blows towards the north Indian Ocean and southern peninsula in both observation and HSM-IAV. But these southerly wind anomalies are absent in LSM-IAV. The unrealistic negative correlation present between SPIRF and Nino3.4 SST in LSM-IAV can be due to the absence of moisture transport from the Equatorial Indian Ocean through this southerly wind. Unrealistic dry anomalies are also observed over north and south western Indian Ocean in LSM-IAV. But the observed wet anomalies over western Indian Ocean and dry anomalies over eastern Indian Ocean is also better simulated by LSM-IAV. Instead of observed east-west asymmetry in the rainfall anomalies, the HSM-IAV shows a north-south asymmetry in the anomalous rainfall with wet bias in the north of the equator including southern peninsular India and dry bias in south except its western edge (40°E-50°E). These type of north-south rainfall anomalies can be related to the changes in Hadley circulation rather than Walker circulation. So, the analysis of the modulation of Hadley circulation by El Nino in the models will be able to explain this north-south asymmetry in the anomalous rainfall pattern in HSM-IAV. This will be explored in the next section.

The regression of Nino3.4 SST onto SST-wind-rainfall over Pacific Ocean is analysed to understand the unrealistic teleconnection of SPIRF and El Nino in LSM-IAV. Anomalous SST gradient is observed over the north western Pacific Ocean due to the warm SST anomalies over South China Sea and clod SST anomalies over Philippian Sea. This pattern is absent in LSM-IAV. Due to these biases in SST anomalies, observed anticyclonic circulation over South China Sea is altered in LSM-IAV, which might be an important source of error that leads to an incorrect SPIRF-Nino3.4 SST relationship in LSM-IAV models. To confirm this, we need to check how El Nino modulates Walker circulation in Indian Ocean in actual observation as well as in low skill and high skill models.

Positive rainfall anomalies over the south western Indian Ocean associated with PIOD is simulated correctly in both LSM-IAV and HSM-IAV model ensembles (Fig.8). Both the ensembles were able to capture the anomalous positive rainfall over north western Indian Ocean present during PIOD. Similar to El Nino, LSM-IAV could not capture the positive rainfall anomalies over the southern peninsular India. HSM-IAV ensemble well captured the positive rainfall anomalies over the north western Indian Ocean and adjoining land areas including southern peninsular India. During PIOD, positive rainfall anomalies are observed over Bay of Bengal which is contradictory to the observation.

5. Modulation Of Hadley And Walker Circulation During El Nino And Piod In Cmip5 Models

The modulation of Hadley and Walker circulation by El Nino and PIOD is studied by analysing the regression maps of Nino3.4 SST and DMI onto the Walker and Hadley circulation. Observational analysis reveals that El Nino is associated with the ascending anomalies over the entire latitudes (30°S to 30°N) of western Indian Ocean and southern peninsular India (Fig. 9). The anomalous SST and rainfall patterns reveal that the entire western Indian Ocean is warm and wet during El Nino. The strong ascending

anomalies are observed in the 5°N-10°N (60°E-85°E) latitude region, where the strong positive rainfall anomalies are also observed (Fig.9).

The El Nino related ascending anomalies over north western Indian Ocean and southern peninsular India is better simulated in HSM-IAV. This leads to a better simulation of rainfall anomalies over southern Peninsular India and Arabian Sea. Strong descending anomalies are observed over the central Indian Ocean in HSM-IAV, which is not present in the observation. This can be linked to the unrealistic cold SST anomalies in the central Indian Ocean in HSM-IAV. These modulations of Hadley circulation are responsible for the north-south asymmetry in the rainfall anomalies in HSM-IAV.

In LSM-IAV, unrealistic descending anomalies to the north (10°N-15°N) and south of the equator (10°N-10°S) are noticed. El Nino related anomalous warming over the central and eastern Equatorial Indian (5°S-5°N) Ocean in LSM-IAV is associated with these descending anomalies. This abnormal warming and descending anomalies are not present in the actual observation. These descending wind anomaly leads to an erroneous dry bias over the northern and southern latitudes of Indian Ocean (Fig.7). The abnormal warming of the central and eastern Equatorial Indian Ocean and the unrealistic westward extension of warm anomalies over the equatorial Pacific cold tongue region during El Nino is simultaneously coexisting in the LSM-IAV. These two abnormalities are absent in HSM-IAV suggest that these abnormalities may be directly or indirectly linked and is responsible for the modulation of Hadley circulation over the western Indian Ocean and southern peninsular India (60°E-85°E) in LSM-IAV models.

Compared to Nino3.4 SST regression onto Hadley circulation, a very similar but more intense pattern is observed for the regression of DMI onto Hadley cell circulation in actual observation and also in LSM-IAV and HSM-IAV model ensembles. Since the SST, wind and rainfall anomalies associated with PIOD and El Nino over the region of interest (60°E-85°E) is very similar but with more intense anomalies during PIOD, we found a similar but with more intense ascending and descending anomalies for actual observation and models during PIOD (Fig.10).

The east-west asymmetry of Indian and Pacific Ocean warming during El Nino leads to a modulation in the Walker circulation over these regions. We have analysed regression maps of Walker circulation over equatorial (5°S-5°N) and northern (5°N-15°N) latitudes. Anomalous ascending motion over the central and eastern Pacific Ocean (East of 160°E) and western Indian Ocean (west of 80°E) where we found the positive SST and rainfall anomalies and anomalous descending motion over the western Pacific and eastern Indian Ocean where we found the negative SST and rainfall anomalies are seen in the equatorial (5°S-5°N) Walker circulation in the actual observation (Fig.11). This pattern is not well simulated in HSM-IAV with under estimated ascending anomalies over the central Pacific Ocean and abnormal descending anomalies over the western Indian Ocean except over 40°E-50°E longitudes where the upward motion and rainfall anomalies are similar to the observation. In LSM-IAV, the ascending anomalies over the Equatorial Pacific Ocean is shifted more westwards (up to 140°E) due to the westward extension of cold tongue. The ascending motion in the western Indian Ocean is better simulated in LSM-IAV rather than in HSM-IAV.

Compared to El Nino, a similar but more intense ascending anomalies over the central and eastern Pacific Ocean and western Indian Ocean and descending anomalies over the western Pacific and eastern Indian Ocean is observed in the actual observation as well as in the model ensembles during PIOD. LSM-IAV shows a westward extension of ascending anomalies over Pacific and HSM-IAV shows abnormal descending anomalies over the central Indian Ocean (Fig.12). Modulation of EquatorialWalker circulation by El Nino and PIOD is not enough to explain the observed and simulated SPIRF-Nino3.4 and SPIRF-DMI direct relationship.

To explain how the modulation of the Walker circulation which affects SPIRF during El Nino in CMIP5 models, we have analysed the regression maps of Nino3.4 SST on to the Walker circulation over the northern latitudes 5°N-15°N (Fig.13). Over Pacific Ocean, El Nino is related to the strong descending anomalies over 100°E-140°E region where we find the South china Sea anticyclonic circulation. This anticyclonic circulation is associated with the reversal of vertical motion over Indian Ocean from downward to upward during the mid of October (Watanabe et al. 2002). In the actual observation, we find another anticyclonic circulation over Bay of Bengal and hence weak descending anomalies over this region (5°N-15°N,80°E-100°E) and ascending anomalies over the western Indian Ocean and southern Peninsular India (40°E-80°E). Thus, the establishment of South China Sea anticyclone and Bay of Bengal anticyclone are related to El Nino. The ascending anomalies related to the Bay of Bengal anticyclone in responsible for the above normal rainfall over southern peninsular India. The descending anomalies over South China Sea and ascending anomalies over Indian Ocean (50°E-80°E) is well captured but with lower intensity in HSM-IAV. But the observed Bay of Bengalanticyclonic circulation is not simulated correctly by HSM-IAV ensemble. Instead of observed descending anomalies and negative rainfall anomalies, HSM-IAV shows positive rainfall anomalies over Bay of Bengal.

The observed anticyclonic circulation over South China Sea is shifted more westward in LSM-IAV as manifested by the westward shifted descending anomalies (Fig.13b). The anticyclonic circulation over the Bay of Bengal is correctly simulated by LSM-IAV. But this anticyclonic circulation extended more westward and hence simulated unrealistic descending anomalies over southern Peninsular India and is extended up to 70°E. Due to this ascending motion, the southern peninsular India is dry during El Nino in LSM-IAV models. Thus, the modulation of the South China Sea anticyclone by the westward extended cold tongue in CMIP5 models can be responsible for the unrealistic negative correlation observed between SPIRF and Nino3.4 SST in most of the CMIP5 models. Compared to El Nino, a similar but more intense pattern of northern Walker circulation for observation and model ensemble is observed during PIOD (Fig.14).

6. Summary And Conclusion

The skill of 34 CMIP5 models to simulate the mean state and interannual variability of northeast monsoon rainfall over southern Peninsular India is discussed in this paper. The models captured the mean northeast monsoon rainfall over the Indian Ocean and southern peninsular India (10°S-30°N,40°E-120°E) reasonably well with a pattern correlation ranging from 0.6 to 0.93 and RMSE between 1.73 and

3.83. We noticed that a few individual models have outperformed the multi model ensemble. The high skill (HSM) and low skill models (LSM) are selected based on the ratio of PCC to RMSE and its ensembles are studied. A strong wet bias over the south western Indian Ocean and dry bias over south eastern Indian Ocean, south Bay of Bengal and southern Peninsular India in the mean northeast monsoon rainfall is observed in CMIP5 models. Over Indian Ocean, a positive IOD like Indian Ocean warming bias exist in LSM and a negative IOD like Indian Ocean warming bias exist in HSM. Over Pacific Ocean, La Nina like SST bias is observed in both the ensembles, which is more intense in HSM compared to LSM.

In LSM, a warm SST bias over the western Indian Ocean and the absence of equatorial westerlies over the Indian Ocean led to the unrealistic convergence and ascending wind anomalies over south western Indian Ocean. A cold bias in the northern Arabian Sea and warm bias in the western equatorial Indian Ocean in LSM leads to a strong north-south SST gradient in western Indian Ocean. This also causes variations in Hadley circulation which shows an unrealistic ascending (descending) motion over the western equatorial Indian Ocean (Arabian Sea and the southern Peninsular India). So, the LSM models shows a wet bias over western Indian Ocean and dry bias over Arabian Sea and southern peninsular India. In LSM, PIOD like east-west asymmetry in the SST bias over Indian Ocean leads to modulation in the Walker circulation which shows an unrealistic ascending motion over the western Indian Ocean. The La Nina like east-west asymmetry in SST bias over the Pacific Ocean is more intense in HSM. Hence an unrealistic descending motion over the central and eastern Pacific Ocean and ascending motion over the western Pacific Ocean is observed in HSM. Generally, the bias in mean rainfall, SST and wind circulation is more intense over the Indian Ocean (Pacific Ocean) in LSM (HSM).

The observational analysis reveals that El Nino and PIOD is associated with the anomalous positive SST over the western Indian Ocean, north equatorial Indian Ocean and equatorial central and eastern Pacific Ocean. El Nino and PIOD is also related to the anomalous negative SST over the south eastern Indian Ocean, western Pacific Ocean and northern and southern central Pacific Ocean. SST and rainfall anomalies are found to be roughly collocated in Indian and Pacific Ocean. Excess rainfall over the southern Peninsular India and deficient rainfall over Maritime continents and South East Asia is observed during El Nino and PIOD years. Strong easterly anomalies over the equatorial Indian Ocean due to the east-west SST gradient and southerly anomalies due to the north-south SST gradient (cold south eastern Indian Ocean and warm north Indian Ocean) are responsible for more moisture transport to the southern Peninsular India from the surrounding Indian Ocean during El Nino and PIOD.

Observational analysis reveals that ascending anomalies are present over warm pool in the climatological mean Walker circulation during NEM season. This is modified as ascending anomalies to the east and west of warm pool region and descending anomalies over warm pool region during El Nino and PIOD. This modulation is manifested as an interesting pattern of warm and wet western Indian Ocean, southern Peninsular India and central and eastern Pacific Ocean and cool and dry warm pool region including Maritime continents.

During El Nino and PIOD years, a gradient in SST is present over the north western Pacific Ocean due to the warm SST anomalies over the South China Sea and clod SST anomalies over the Philippian Sea. This is related to the anticyclonic circulation and strong descending anomalies over the South China Sea. This anticyclonic circulation is associated with the reversal of vertical motion over the Indian Ocean from downward to upward during the mid of October (Watanabe et al. 2002). Here, we find another anticyclonic circulation over the Bay of Bengal. Due to the presence of these anticyclonic circulations, weak descending anomalies are observed over the South BoB (5°N-15°N,80°E-100°E) and ascending anomalies are observed over the western Indian Ocean and southern peninsular India (40°E-80°E). Thus, the establishment of the South China Sea anticyclone and the Bay of Bengal anticyclone during El Nino and PIOD are strongly related with the ascending motion over south peninsular India and hence enhances the south Peninsular Indian rainfall during NEM season.

Above normal SPIRF during El Nino and PIOD is better simulated by a set of models (HSM-IAV) which shows positive CC between SPIRF and Nino3.4 SST as well as SPIRF and DMI. Instead of the observed El Nino and PIOD related east-west asymmetry in Indian ocean rainfall, HSM-IAV model ensemble shows a north-south asymmetry in Indian Ocean rainfall (wet anomalies over the Bay of Bengal and dry anomalies over the central Indian Ocean). In HSM-IAV, an unrealistic cold bias over the equatorial eastern and central Indian Ocean and warm bias over the south eastern Indian Ocean is observed. This modulates the actual Hadley circulation. Strong unrealistic descending anomalies over south-central Indian Ocean is observed in HSM-IAV. These descending anomalies are responsible for the abnormal north-south asymmetry in the rainfall anomalies in HSM-IAV.

LSM-IAV models show an erroneous negative CC between SPIRF-Nino3.4 SST and SPIRF-DMI. The LSM-IAV model ensembles were able to simulate the observed El Nino and PIOD related east-west asymmetry in rainfall over Indian Ocean. But the El Nino forced anomalous south easterlies over the equatorial Indian Ocean is better simulated by the HSM-IAV while the wind anomalies are purely easterlies in LSM-IAV. The absence of southerly component of wind and unrealistic descending motion over the southern Peninsular India in LSM-IAV leads to the erroneous dry anomalies over southern Peninsular India during El Nino and PIOD.

El Nino and PIOD related warm SST anomalies over the equatorial Pacific cold tongue is found to be extended more westward in LSM-IAV. Unrealistic cold SST anomalies over the South China Sea is also observed in the LSM-IAV. Related to these errors, westward extension in the ascending motion over the equatorial Pacific Ocean is observed in the equatorial Walker circulation. Along with the westward extension of cold tongue, the observed El Nino and PIOD related anticyclonic circulation over both the South China Sea and Bay of Bengal is also found to be shifted more westward. This is manifested by the unrealistic westward shifting of descending anomalies up to 70°E (5°N-15°N) in LSM-IAV. Thus, the descending anomalies over the north western Indian Ocean and southern Peninsular India causes erroneous dry anomalies over southern peninsular India and negative CC between SPIRF and Nino 3.4 SST as well as SPIRF and DMI in LSM-IAV. The descending anomalies over South China Sea and ascending anomalies over the western Indian Ocean and southern Peninsular India (50°E-80°E) is well

captured but with lower intensity in HSM-IAV and hence it shows the observed positive CC between SPIRF and Nino3.4 SST as well as SPIRF and DMI.

Declarations

Acknowledgments

One of the authors (SPP) is thankful to UGC for providing fund through DSKPDF. We are grateful to Dr. M. Rajeevan and K. Rajeevan for their valuable suggestions. We acknowledge the World Climate Research Programme's Working Group on coupled modelling which is responsible for CMIP and we thank the climate modelling groups for producing and making available their model output.

Funding: One of the authors (Sreekala P P) is supported financially by UGC through DSKPDF.

Conflicts of interest/Competing interests: Not Applicable

Availability of data and material: Available

Code availability: Available

Authors' contributions: First author have done the analysis and writing part. Both second and third authors actively participated in the research discussions.

Ethics approval: Not Applicable

Consent to participate: Not Applicable

Consent for publication: Not Applicable

References

Acharya N, Kar SC, Kulkarni MA, Mohanty UC, Sahoo LN (2011a) Multimodel ensemble schemes for predicting northeast monsoon rainfall over peninsular India. J Earth Syst Sci 120:795-805

Adler RF, Huffman GJ, Chang A, Ferraro R, Xie P, Janowiak J, Rudolf R, Schneider U, Curtis S, Bolvin D, Gruber A, Susskind J, Arkin P, Nelkin E (2003) The version 2 Global Precipitation Climatology Project (GPCP) monthly precipitation analysis (1979-present). J Hydrometeor 4:1147-1167

Annamalai H, Xie SP, McCreary J P, and Murtugudde (2005) Impact of Indian Ocean sea surface temperature on developing El Nino. J Clim 18:302-319

Archana N, Acharya N, Ankita S, Mohanty UC, Panda TC (2013) On the Predictability of Northeast Monsoon Rainfall over South Peninsular India in General Circulation Models. Pure ApplGeophys 170:1945-1967

Bhanu Kumar OSRU, Naidu CV, Rao SRL (2004) Influence of southern oscillation and SSTs over Nino-3.4 region on the winter monsoon rainfall over coastal Andhra Predesh. Proc Indian Acad Sci 113:313-319

Bin Wang, June-Yi Lee, Baoqiang Xiang (2015), Asian summer monsoon rainfall predictability: a predictable mode analysis. ClimDyn 44:61-74

Bretherton CS, Peters ME, and Back LE (2004), Relationships between water vapor path and precipitation over the tropical Oceans. J. Clim17:1517- 1528

De US, Mukhopadhay RK (1999) The effect of ENSO/Anti ENSO on northeast monsoon rainfall. Mausam 50:343-354

Dhar ON, Rakhecha PR (1983) Forecasting northeast monsoon rainfall over Tamil Nadu, India. Mon Weather Rev111:109-112

Du Y, Xie SP (2008) Role of atmospheric adjustments in the tropical Indian Ocean warming during the 20th century in climate models. Geophys Res Lett35:L08712, doi:10.1029/2008GL033631

Fathrio I, Iizuka S, Manda A, Kodama Y, Ishida S, Moteki Q, Yamada H and Tachibana Y (2017) Assessment of western Indian Ocean SST bias of CMIP5 models. J. Geophys. Res. Oceans **122:** 3123-3140

Feng J, Wang L, Chen W, Fong SK, Leong KC (2010)Different impacts of two types of Pacific Ocean warming on Southeast Asian rainfall during boreal winter. J Geophys Res Atmos 115(24): 1- 9, doi: 10.1029/2010JD014761

Gadgil, S, Gadgil, S (2006) The Indian monsoon, GDP and agriculture. Economic and Political Weekly, XLI, 4887-4895

Girishkumar MS, Thanga Prakash VP, Ravichandran M (2015) Influence of Pacific Decadal Oscillation on the relationship between ENSO and tropical cyclone activity in the Bay of Bengal during October-December. ClimDyn 44:3469-3479

Huffman GJ, Adler RF, Arkin PA, Chang A, Ferraro R, Gruber A, Janowiak J, McNab A, Rudolf B, Schneider U (1997) The global precipitation climatology project (GPCP) combined precipitation dataset. Bull Am Meteorol Soc 78:5-20

Kripalani RH, Kumar P (2004) Northeast monsoon rainfall variability over south peninsular India vis-a-vis the Indian Ocean dipole mode. Int J Climatol 24:1267-1282

Kumar P, Rupa Kumar K, Rajeevan M, Sahai AK (2007) On the recent strengthening of the relationship between ENSO and northeast monsoon rainfall over South Asia. ClimDyn 28:649-660

Li G, Du Y, Xu H, Ren B (2015) An intermodel approach to identify the source of excessive equatorial Pacific cold tongue in CMIP5 models and uncertainty in observational datasets. J Clim 28:7630-7640

Li G, Xie SP (2012) Origins of tropical-wide SST biases in CMIP multimodel ensembles. Geophys Res Lett 39: L22703. doi:10.1029/2012GL053777

Li JP, Feng J (2017) Tropical large-scale atmospheric interaction in association with subtropical aridity trend. In: Fu CB, Mao HT (eds) Aridity trend in Northern China. World Scientific, Singapore

Lindzen RS, Nigam S (1987) On the role of sea surface temperature gradients in forcing low-level winds and convergence in the Tropics. J Atmos Sci 44:2418-2436

Menon A, Levermann A, Schewe J, Lehmann K, Frieler K (2013) Consistent increase in Indian monsoon rainfall and its variability across CMIP-5 models. Earth Sys Dynam 4:287-300

Meyers G, McIntosh P, Pigot L, Pook M (2007) The years of El Niño, La Niña, and interactions with the tropical Indian Ocean. J Clim20:2872- 2880

Nageswara Rao G (1999) Variations of the SO relationship with summer and winter monsoon rainfall over India: 1872-1993. J Climate 12:3486-3495

Neelin JD, Peters O, and Hales K (2009) The transition to strong convection. J Atmos Sci, 66:2367-2384, doi:10.1175/2009JAS2962.1

O'Brien JJ, Hurlburt HE (1974) An equatorial jet in the Indian Ocean: Theory, Science, 184:1075-1077

Parthasarathy B, Munot AA, Kothawale DR (1994) All-India monthly and seasonal rainfall series: 1871-1993. TheorApplClimatol 49:217-224

Prasanna K, Chowdary JS, Naidu CV, Gnanaseelan C, Anant Parekh (2020) Diversity in ENSO remote connection to northeast monsoon rainfall in observations and CMIP5 models. TheorApplClimatol 141:827-839

Prasanna K, Singh P, Chowdary J, Naidu C, Parekh A, GnanaseelanC,Dandi R (2019) Northeast monsoon rainfall variability over the southern Peninsular India associated with multiyear La Niña events. ClimDyn 53(9-10):6265-6291

Raj YEA, Sen PN and Jamadar SM (1993) Outlook on northeast monsoon rainfall of Tamil Nadu. Mausam 44:19-22

Raj YEA, Suresh R, Sankaran PV, Amudha B (2004) Seasonal variation of 200 hPa upper tropospheric features over India in relation to performance of Indian Southwest and Northeast monsoons. Mausam 55:269-280

Rajeevan M, Unnikrishnan CK, Bhate J, Niranjan Kumar K, Sreekala PP (2012) Northeast monsoon over India: variability and prediction. MeteorolAppl 19(2):226-236

Rajiv KC, Jaideep J, Jayaraman, Mathangi, Bala G, Ravindranath NH (2012) Multi-model climate change projections for India under representative concentration pathways. Curr Sci 103 (7):791-802

Ramu DA, Chowdary JS, Ramakrishna SSVS, Kumar OSRUB. (2018) Diversity in the representation of large-scale circulation associated with ENSO-Indian summer monsoon teleconnections in CMIP5 models. TheorApplClimatol132:465-478

Rao Krishna PR, Jganathan P (1953) A study of the northeast monsoon rainfall of Tamilnadu. Indian J Meteor Geophys 4:22-43

Rao RR, Sivakumar R (2000) Seasonal variability of near-surface thermal structure and heat budget of the mixed layer of the tropical Indian Ocean from a new global Ocean temperature climatology. J Geophys Res 105:C1995-1015

Raymond DJ (2000) Thermodynamic control of tropical rainfall. Quart. J. Roy. Meteor. Soc 126:889-898

Roy I, Tedeschi R, Collins M (2019) ENSO teleconnections to the Indian summer monsoon in observations and models. Int J Climatol 37(4):1794-1813

Sabeerali CT, Rao SA, Dhakate AR, Salunke K, Goswami BN (2015) Why ensemble mean projection of south Asian monsoon rainfall by CMIP5 models is not reliable? ClimDyn 45:161-174. doi:10.1007/s00382-014-2269-3

Santoso A, Mcphaden MJ, Cai W (2017) The Defining Characteristics of ENSO Extremes and the Strong 2015/2016 El Nino. Rev. Geophys. 55:1079-1129

Schneider EK, Lindzen RS (1977) Axially sym-metric steady state models of the basic state for in-stability and climate studies. Part I. Linear calculations J. Atmos. Sci. 34, 263:279

Schott FA, McCreary JP (2001) The monsoon circulation of the Indian Ocean. Prog. Oceanogr 51:1-123

Schott FA, Xie SP, and McCreary J (2009) Indian Ocean circulation and climate variability, Rev Geophys 47: RG1002 doi:10.1029/2007RG000245, 200

Sengupta A, Sumant N (2019) The Northeast Winter Monsoon over the Indian Subcontinent and Southeast Asia: Evolution, Interannual Variability, and Model Simulations. J Climate32:231-249

Shin DB, Kim JH, Park HJ (2011), Agreement between monthly precipitation estimates from TRMM satellite, NCEP reanalysis and merged gauge-satellite analysis. J Geophys Res 116: D16105. doi:10.1029/2010JD015483

Siew JH, Tangang FT, Juneng L (2014) Evaluation ofCMIP5 coupled atmosphere-Ocean general circulation models and projection of the Southeast Asian winter mon-soon in the 21st century. Int. J. Climatol 34:2872–2884

Singh N Sontakke NA (1999) On the variability and prediction of postmonsoon season rainfall over India. Int J Climatol 19:309-339

Sreekala PP, Rao SV, Rajeevan K, Arunachalam MS (2018) Combined effect of MJO, ENSO and IOD on the intraseasonal variability of northeast monsoon rainfall over South Peninsular India. ClimDyn 51: 3865-3882.https://doi.org/10.1007/s00382-018-4117-3

Sreekala PP, Rao SV, Rajeevan M (2012) Northeast monsoon rainfall activity over South Peninsular India and its teleconnections. TheorApplClimatol108:73-83

Suppiah R (1996) Spatial and temporal variations in the relationship between southern oscillation phenomenon and the rainfall of Sri Lanka. Int J Climatol 16:1391-1407

Suppiah R (1997) Extremes of southern oscillation phenomenon and the rainfall of Sri Lanka. Int J Climatol 17:87-101

Taylor KE (2001) Summarizing multiple aspects of model performance in a single diagram. J Geophys Res 106:7183-7192

Taylor KE, Stouffer RJ, Meehl GA (2012) An overview of CMIP5 and the experiment design. Bull Am Meteorol Soc 90:485-498

Wang B, Wu R, Fu X (2000)Pacific-East Asian teleconnection: how does ENSO affect East Asian climate? J. Clim. 13(9): 1517- 1536

Watanabe M, Kimoto M, Jin FF (2002) Role of Indian Ocean warming in the development of the Philippine Sea anticyclone during El Nino. Geophys. Res. Lett 29:1478, doi:10.1029/2001GL014318.

Xie P, Janowiak JE, Arkin PA, Adler RF, Gruber A, Ferraro R, Huffman GJ, Curtis S (2003) GPCP pentad precipitation analyses: An experimental dataset based on gauge observations and satellite estimates. J. Climate 16:2197-2214

Yadav RK (2012) Why is ENSO influencing Indian northeast monsoon in the recent decades? Int J Climatol 32:2163-2180

Yadav RK (2013) Emerging role of Indian Ocean on Indian Northeast monsoon. ClimDyn 41:105-116

Zhang R, Sumi A, Kimoto M (1996) Impact of El Niño on the East Asian monsoon: a diagnostic study of the '86/87 and '91/92 events. J. Meteorol. Soc. Jpn74(1): 49-62

Zheng Y, Lin JL, Shinoda T (2012) The equatorial Pacific cold tongue simulated by IPCC AR4 coupled GCMs: upper Ocean heat budget and feedback analysis. J Geophys Res 117:C05024. https ://doi.org/10.1029/2011J C0077 46

Zubair L, Ropelewski CF (2006) The strengthening relationship between ENSO and northeast monsoon rainfall over Sri Lanka and southern India. J Clim 19:1567-1575

Tables

Table 1 A list of 34 CMIP5 models used in this study

Sl No.	Institute ID	Model Name	Atmospheric Grid	
			Latitude	Longitude
1	CSIRO-BOM	ACCESS1.0	1.25	1.875
2	CSIRO-BOM	ACCESS1.3	1.25	1.875
3	BCC	BCC-CSM1.1	2.7906	2.8125
4	NCAR	CCSM4	0.9424	1.25
5	CMCC	CMCC-CESM	3.4431	3.75
6	CMCC	CMCC-CM	0.7484	0.75
7	CMCC	CMCC-CMS	3.7111	3.75
8	CNRM- CERFACS	CNRM-CM5	1.4008	1.40625
9	CNRM- CERFACS	CNRM-CM5-2	1.4008	1.40625
10	CSIRO-QCCCE	CSIRO-Mk3.6.0	1.8653	1.875
11	CCCMA	CanCM4	2.7906	2.8125
12	CCCMA	CanESM2	2.7906	2.8125
13	LASG-CESS	FGOALS-g2	2.7906	2.8125
14	LASG-IAP	FGOALS-s2	1.659	2.8125
15	NOAA GFDL	GFDL-CM2.1	2.0225	2.5
16	NOAA GFDL	GFDL-CM3	2	2.5
17	NOAA GFDL	GFDL-ESM2G	2.0225	2
18	NOAA GFDL	GFDL-ESM2M	2.0225	2.5
19	NASA GISS	GISS-E2-R	2	2.5
20	NASA GISS	GISS-E2-R-CC	2	2.5
21	MOHC	HadCM3	2.5	3.75
22	MOHC	HadGEM2-CC	1.25	1.875
23	MOHC	HadGEM2-ES	1.25	1.875
24	INM	INM-CM4	1.5	2
25	IPSL	IPSL-CM5A-LR	1.8947	3.75
26	IPSL	IPSL-CM5A-MR	1.2676	2.5
27	MIROC	MIROC-ESM	2.7906	2.8125

28	MIROC	MIROC-ESM-CHEM	2.7906	2.8125
29	MIROC	MIROC5	1.4008	1.40625
30	MIROC	MIROC4	1.4008	1.40625
31	MPI-M	MPI-ESM-LR	1.8653	1.875
32	MPI-M	MPI-ESM-MR	1.8653	1.875
33	MRI	MRI-CGCM3	1.12148	1.125
34	NCC	NorESM1-M	1.8947	2.5

Table 2 Pattern correlation, RMSE and its ratio (PCC/RMSE) of mean (1979-2005) NEMR over the region (10°S-30°N,40°E-120°E) simulated in the 34 CMIP5 models

Models	PCC	RMSE	RATIO
MRI-CGCM3	**0.61**	**3.39**	**0.18**
ACCESS1.3	**0.67**	**3.67**	**0.18**
CMCC-CMS	**0.60**	**3.01**	**0.20**
HadGEM2-CC	**0.66**	**3.32**	**0.20**
HadGEM2-ES	**0.69**	**3.43**	**0.20**
ACCESS1.0	0.74	3.20	0.23
FGOALS-g2	0.68	2.66	0.26
CMCC-CM	0.70	2.71	0.26
INM-CM4	0.76	2.83	0.27
GISS-E2-R-CC	0.78	2.75	0.28
GISS-E2-R	0.79	2.73	0.29
MIROC4	0.74	2.44	0.30
FGOALS-s2	0.74	2.40	0.31
BCC-CSM1.1	0.76	2.39	0.32
GFDL-CM3	0.78	2.38	0.33
CSIRO-Mk3.6.0	0.88	2.64	0.33
HadCM3	0.85	2.33	0.37
NorESM1-M	0.80	2.16	0.37
IPSL-CM5A-MR	0.83	2.18	0.38
CNRM-CM5	0.81	2.08	0.39
CNRM-CM5-2	0.82	2.01	0.41
IPSL-CM5A-LR	0.85	2.05	0.41
CCSM4	0.83	2.01	0.41
MIROC-ESM	0.85	2.01	0.42
GFDL-ESM2M	0.88	1.97	0.44
MIROC-ESM-CHEM	0.87	1.87	0.47
MME	**0.88**	**1.72**	**0.51**
MIROC5	0.88	1.71	0.52

CanCM4	0.90	1.69	0.53
CMCC-CESM	0.89	1.68	0.53
GFDL-CM2.1	**0.92**	**1.69**	**0.54**
GFDL-ESM2G	**0.92**	**1.61**	**0.57**
CanESM2	**0.91**	**1.51**	**0.60**
MPI-ESM-MR	**0.92**	**1.36**	**0.68**
MPI-ESM-LR	**0.93**	**1.35**	**0.69**

Table 3 Correlation coefficient between SPIRF and Nino3.4 SST and SPIRF and DMI in the observation and 34 CMIP5 models

Models	Nino3.4	DMI
ACCESS1.0	-0.14	-0.04
ACCESS1.3	-0.01	0.46
BCC-CSM1.1	0.45	0.34
CanESM2	-0.73	-0.57
CanCM4	-0.55	-0.60
CCSM4	-0.65	-0.51
CMCC-CESM	0.19	0.28
CMCC-CM	0.36	0.33
CMCC-CMS	0.28	-0.13
CNRM-CM5	-0.03	-0.07
CNRM-CM5-2	-0.43	-0.37
CSIRO-Mk3.6.0	-0.42	0.19
FGOALS-s2	-0.64	-0.60
FGOALS-g2	-0.53	-0.49
GFDL-CM3	-0.45	-0.62
GFDL-CM2.1	-0.29	-0.23
GFDL-ESM2M	-0.52	-0.34
GFDL-ESM2G	-0.43	-0.31
GISS-E2-R	-0.10	-0.12
GISS-E2-R-CC	0.23	-0.39
HadCM3	-0.25	-0.25
HadGEM2-CC	-0.11	-0.39
HadGEM2-ES	-0.07	-0.06
INM-CM4	-0.37	-0.63
IPSL-CM5A-LR	0.33	0.34
IPSL-CM5A-MR	0.04	-0.13
MIROC5	-0.22	-0.46
MIROC-ESM	0.09	-0.64

MIROC-ESM-CHEM	0.00	0.16
MPI-ESM-LR	-0.08	0.14
MPI-ESM-MR	0.10	0.26
MRI-CGCM3	0.19	0.21
NorESM1-M	-0.33	-0.31
Observation	0.32	0.24

Figures

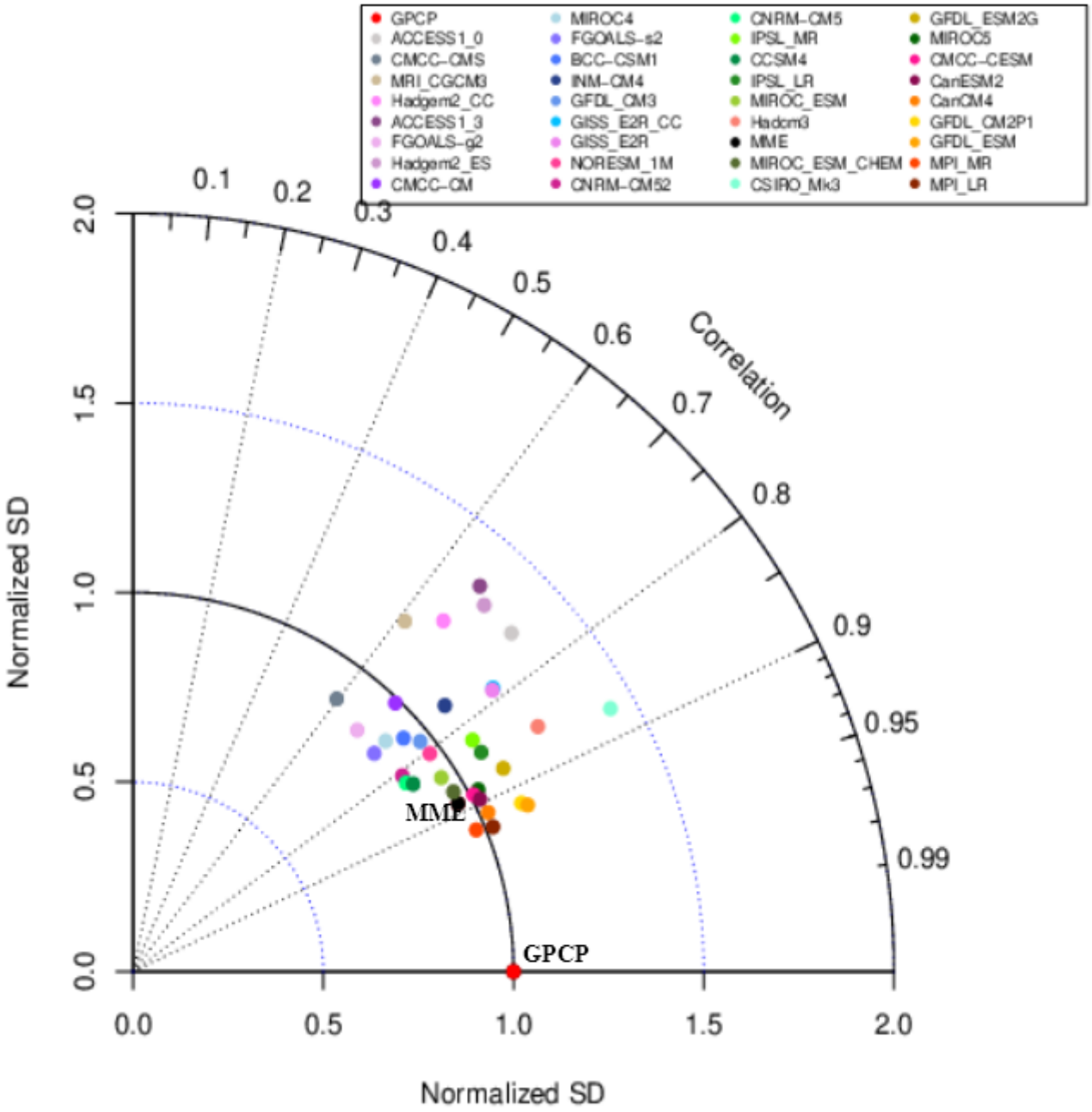

Figure 1

Taylor diagram of the mean northeast monsoon rainfall over the region (10°S-30°N,40°E-120°E) simulated in the CMIP5 models during the period 1979-2005

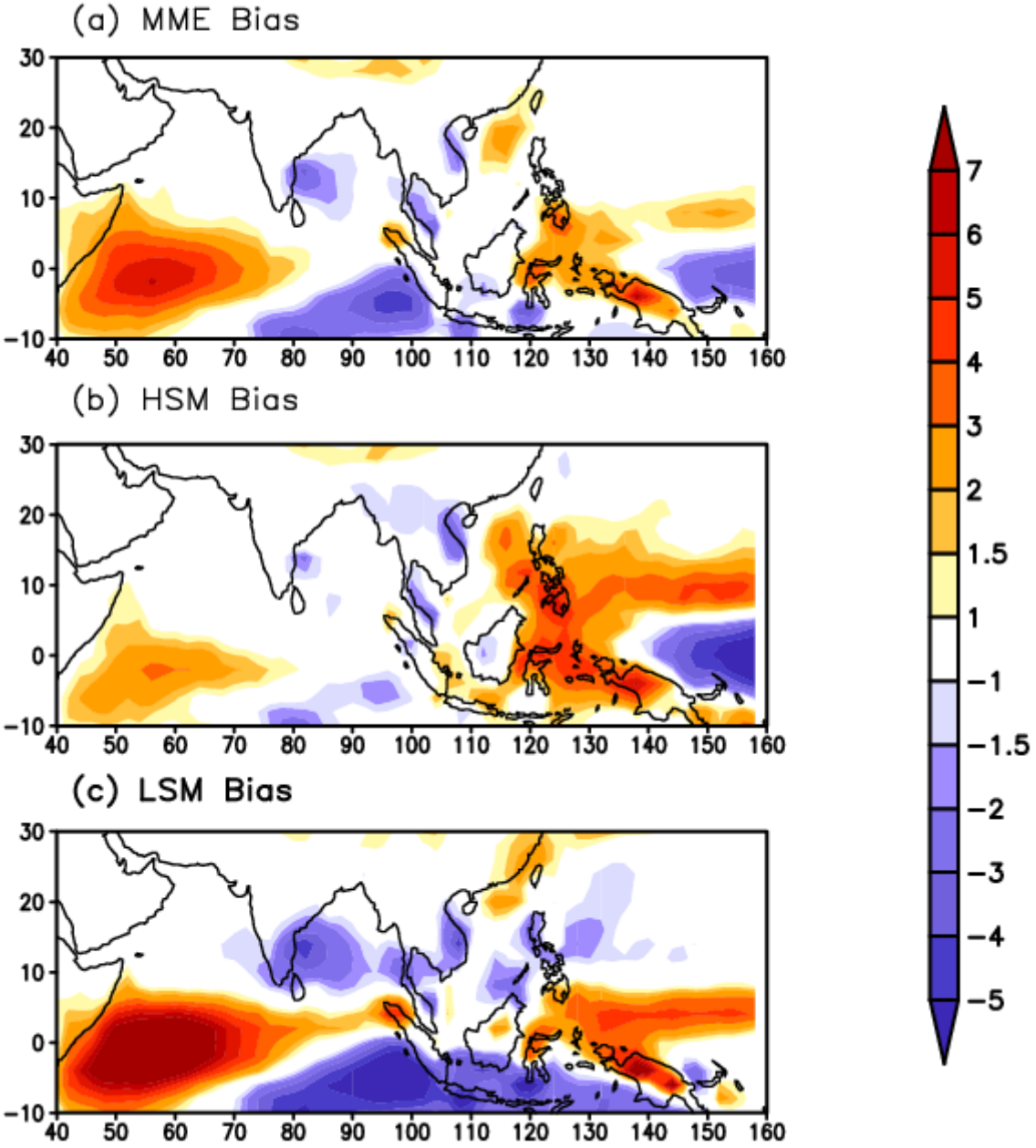

Figure 2

NEM (OND) mean biases in rainfall (mm/day) for (a) Multi model ensemble (b) High skill models ensemble (c) Low skill model ensemble

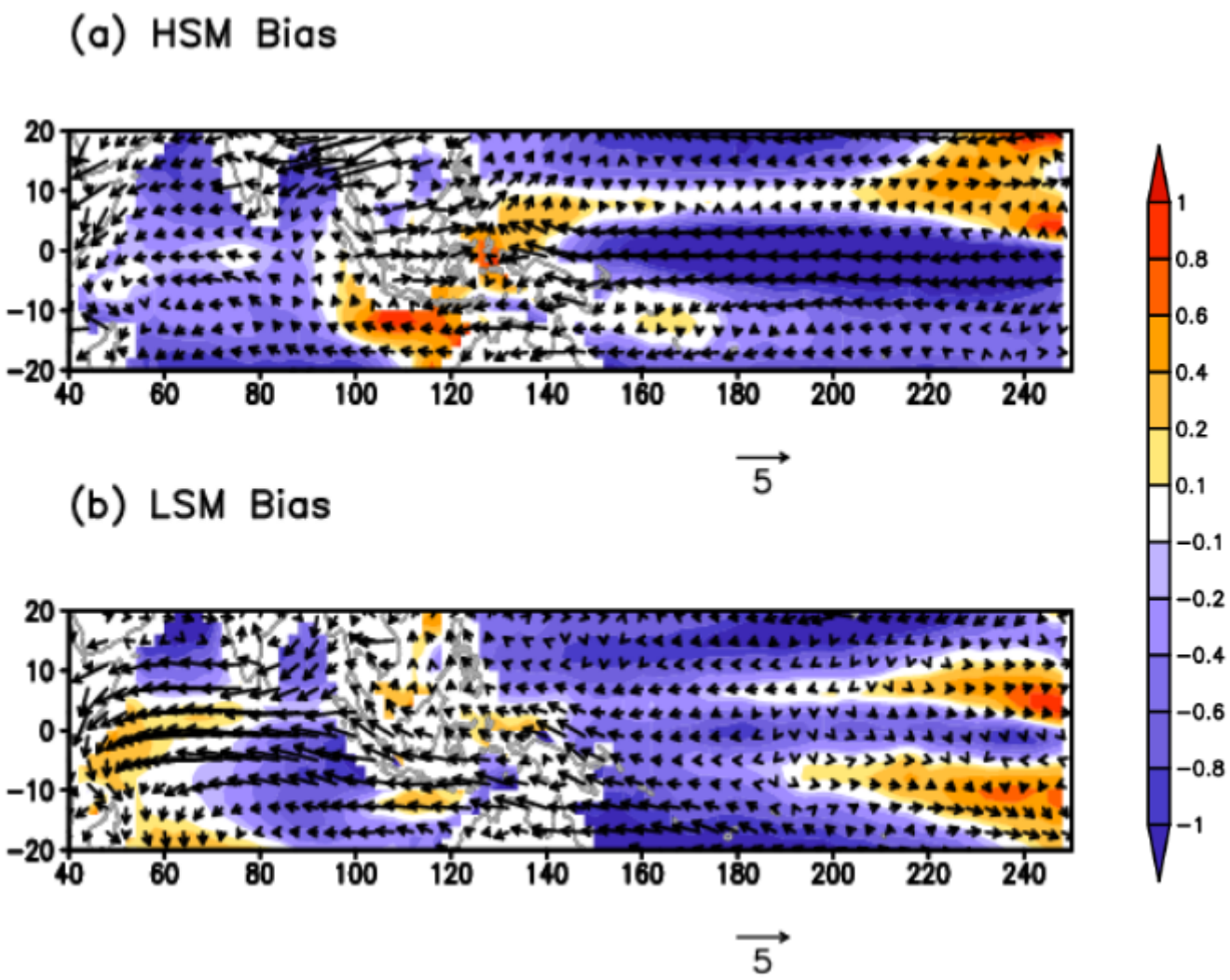

Figure 3

NEM (OND) mean biases in SST (shaded) and 850 hPa wind (vector) for (a) High skill models ensemble (b) Low skill model ensemble

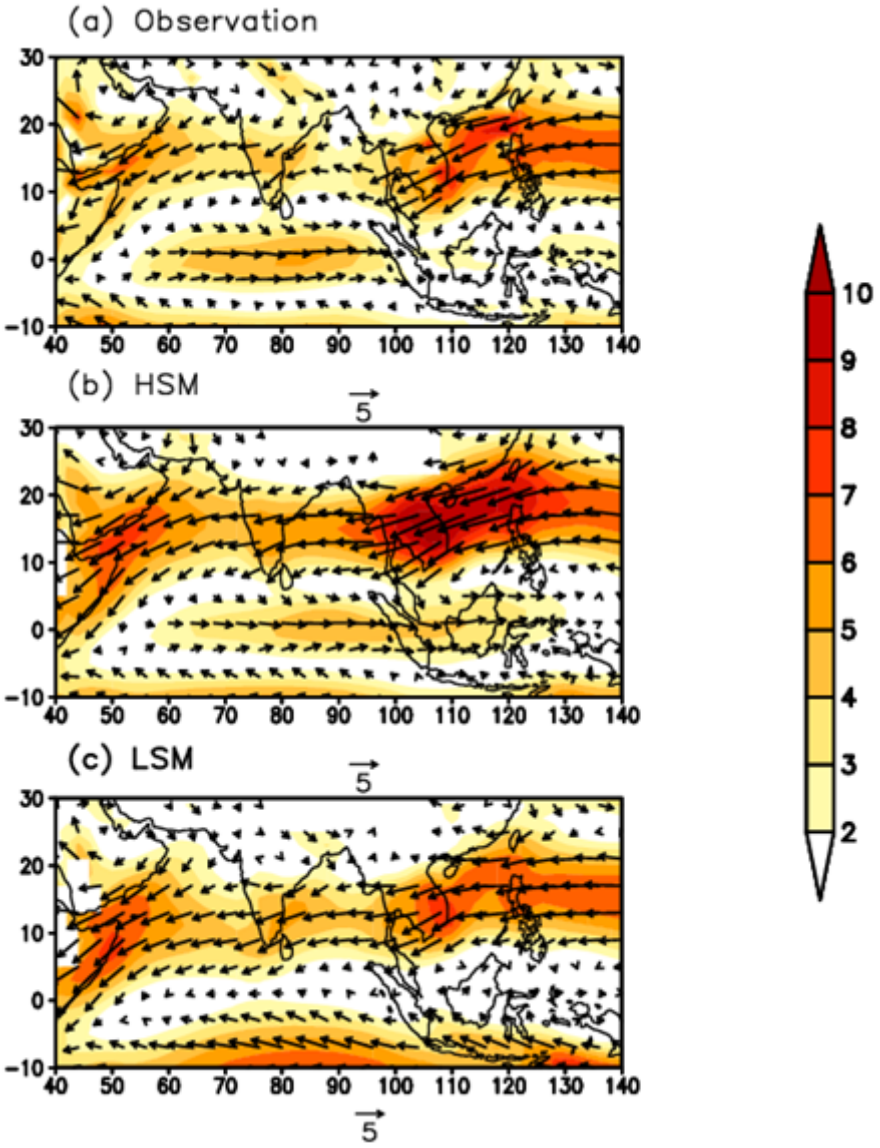

Figure 4

NEM (OND) mean 850 hPa wind (ms-1) for (a) Observation (b) High skill models ensemble (c) Low skill model ensemble

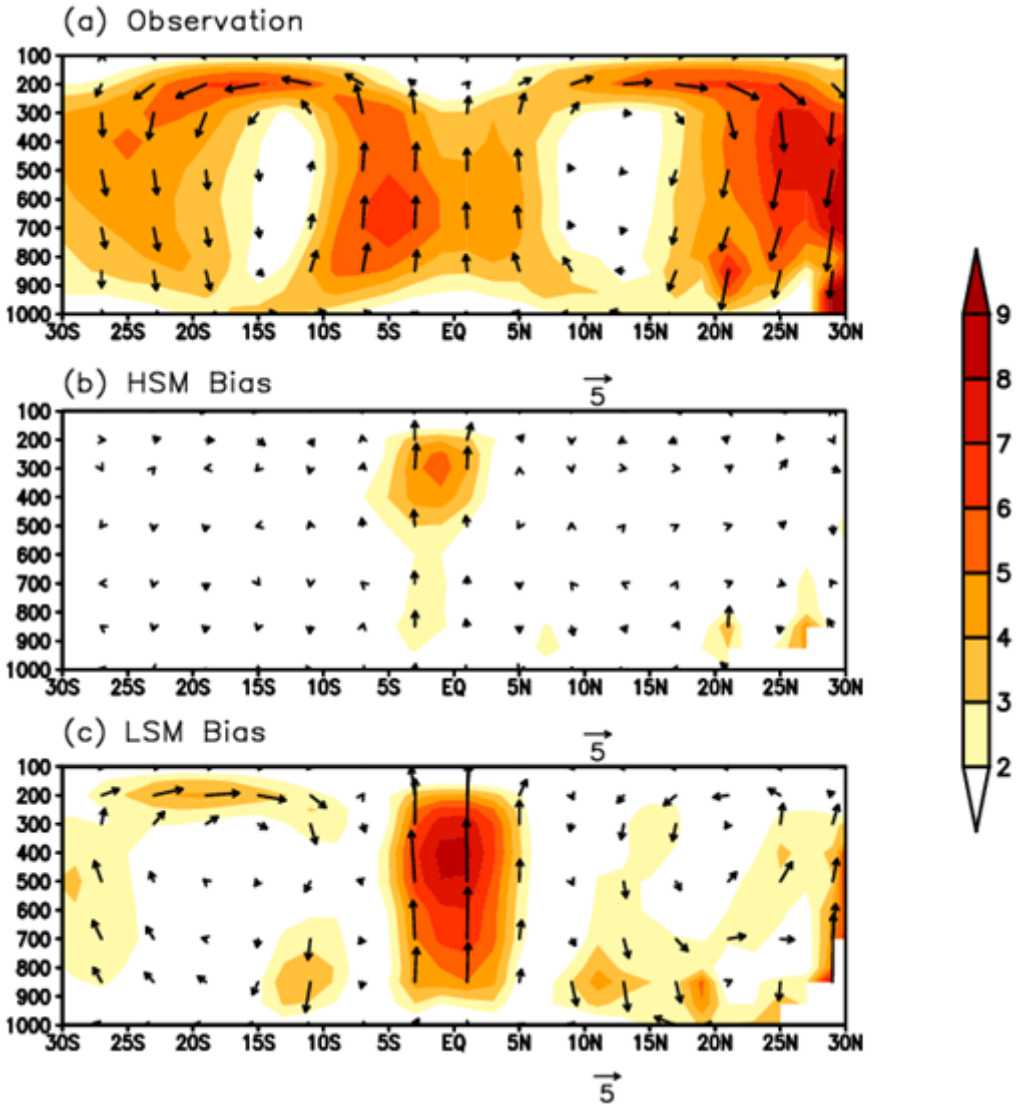

Figure 5

Mean NEM (OND) Hadley circulation (1979-2005) for (a) Observation and bias in Hadley circulation for (b) HSM and (c) LSM

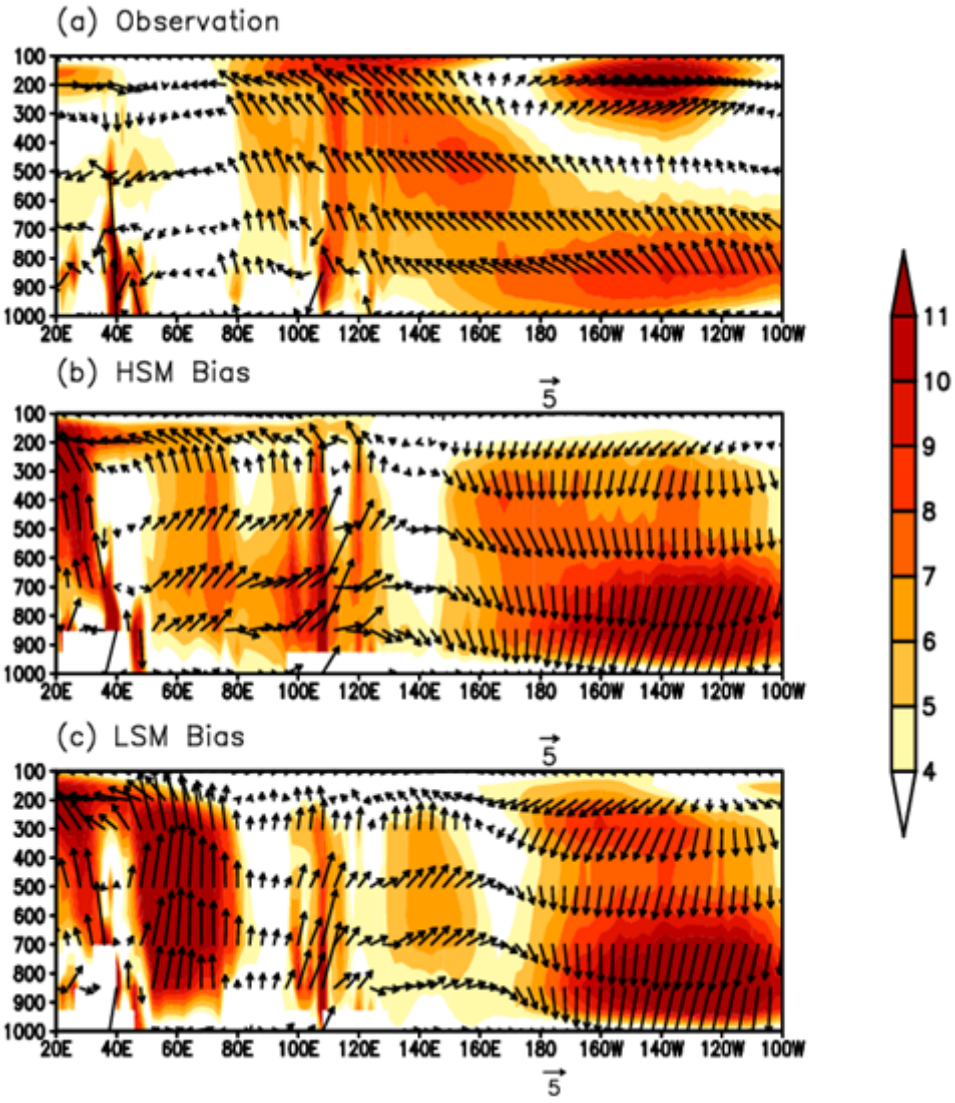

Figure 6

Mean NEM (OND) Walker circulation (1979-05) for (a) Observation and mean bias in Walker cell circulation for (b) HSM and (c) LSM

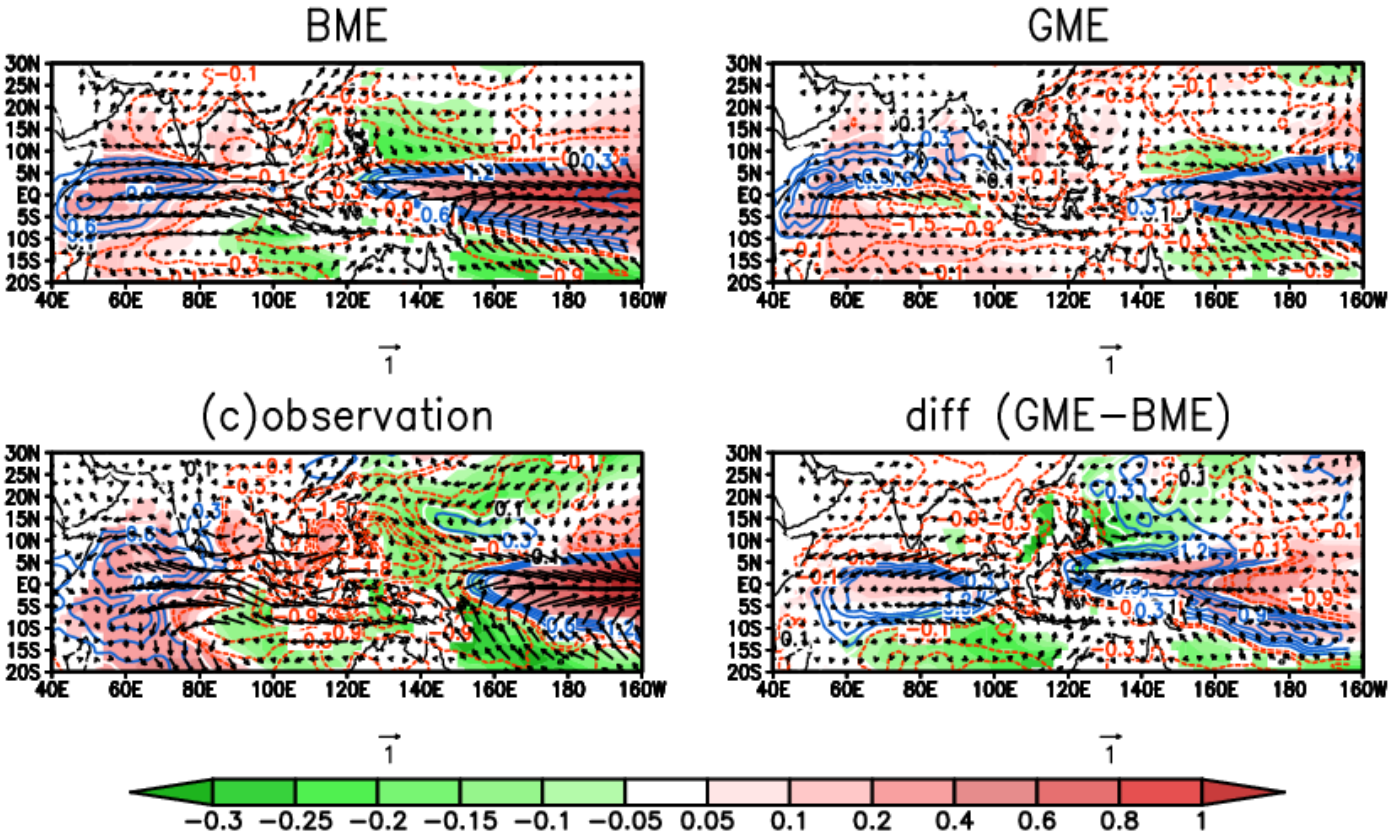

Figure 7

Regression maps of Nino 3.4 SST (OND) onto NEM rainfall (contour blue-positive and red dot line-negative), SST (shaded) and 850 hPa wind (vector) for a period 1979-2005 for (a) LSM (b) HSM (c) Observation and (d) HSM-LSM difference

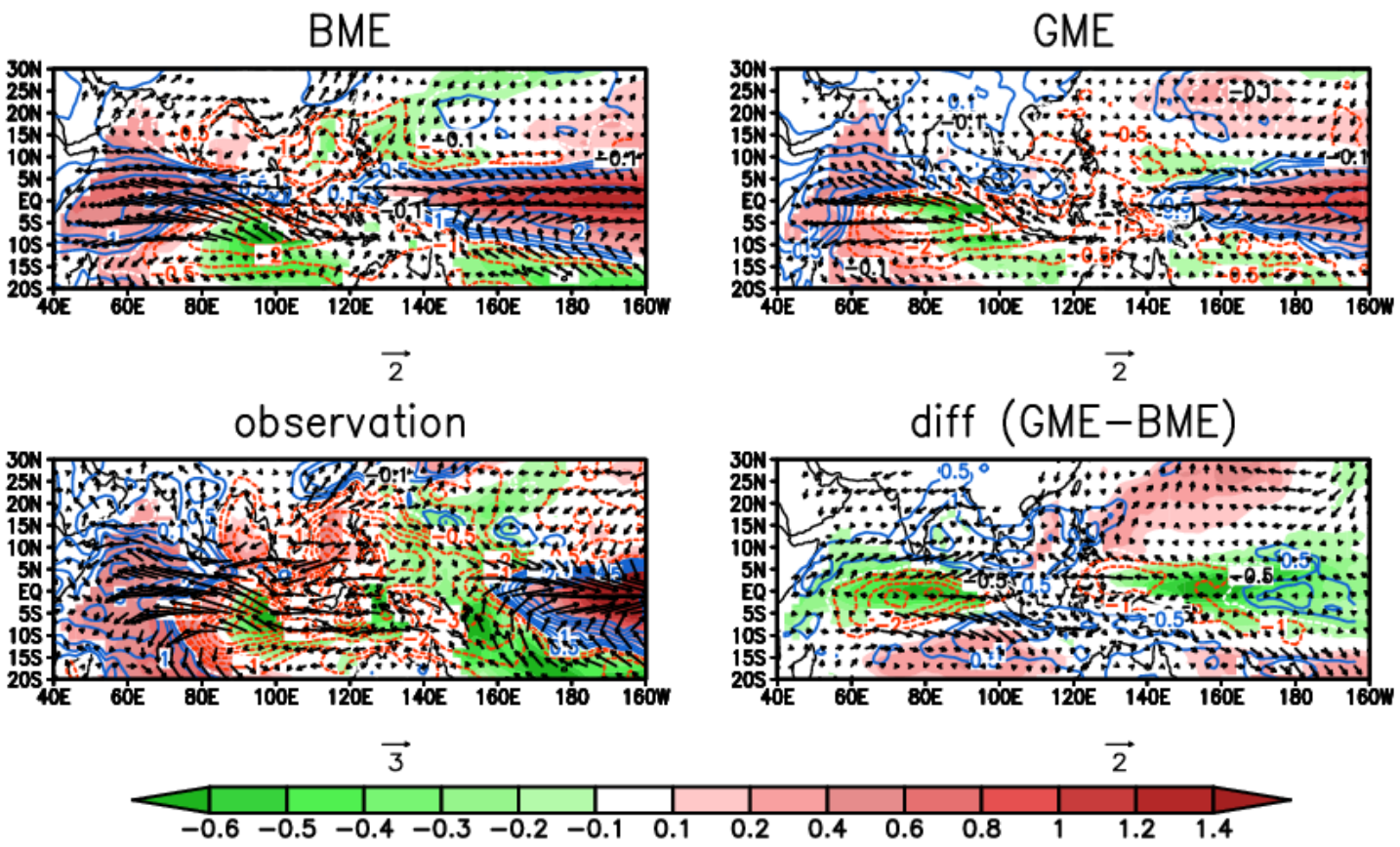

Figure 8

Regression maps of DMI (OND) onto NEM rainfall (contour blue-positive and red dot line-negative), SST (shaded) and 850 hPa wind (vector) for a period 1979-2005 for (a) LSM(b) HSM (c) Observation and (d) HSM-LSM difference

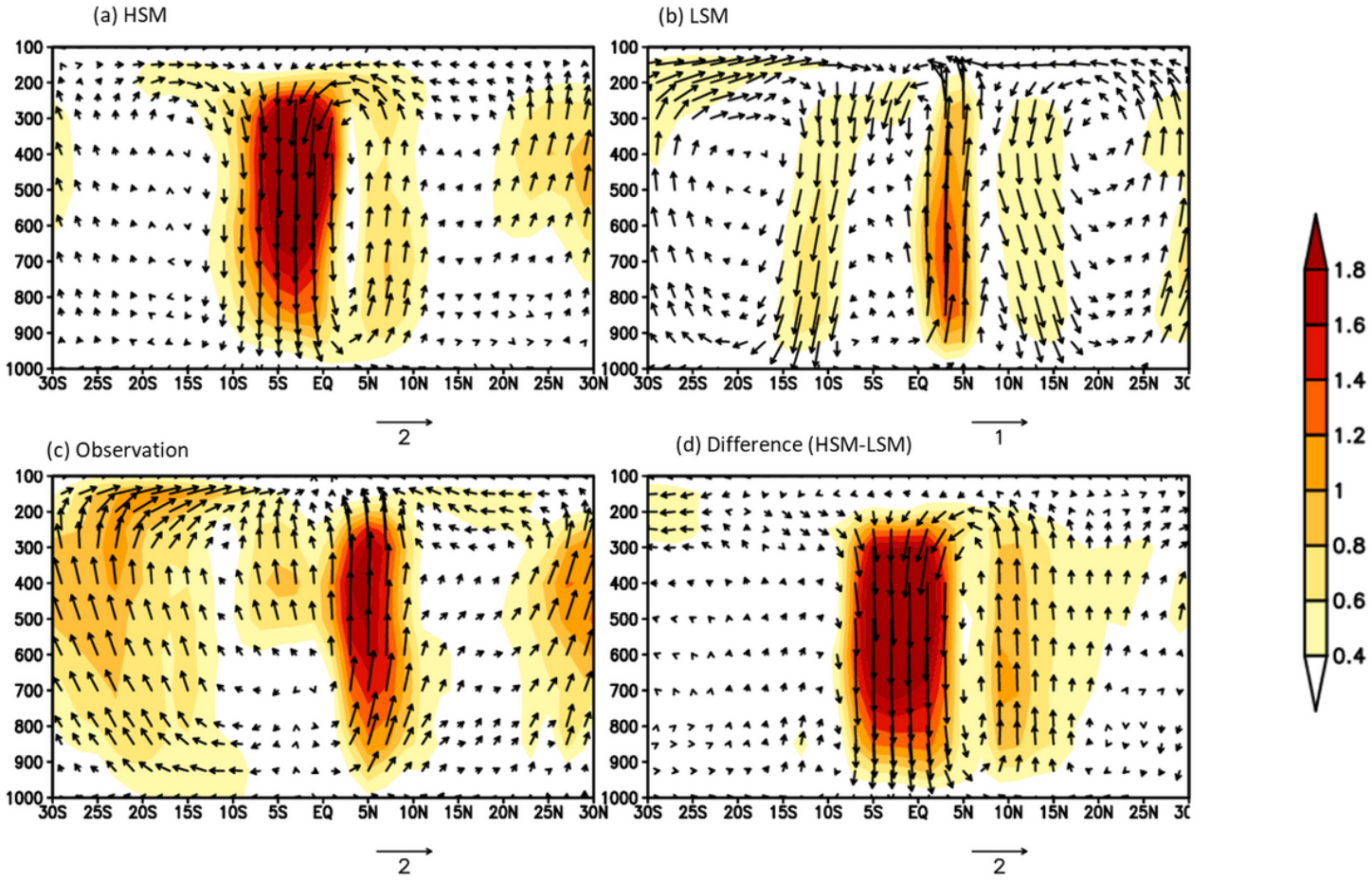

Figure 9

Regression maps of Nino 3.4 SST (OND) onto NEM Hadley circulation for a period 1979-2005 for (a) HSM (b) LSM (c) Observation and (d) HSM-LSM difference

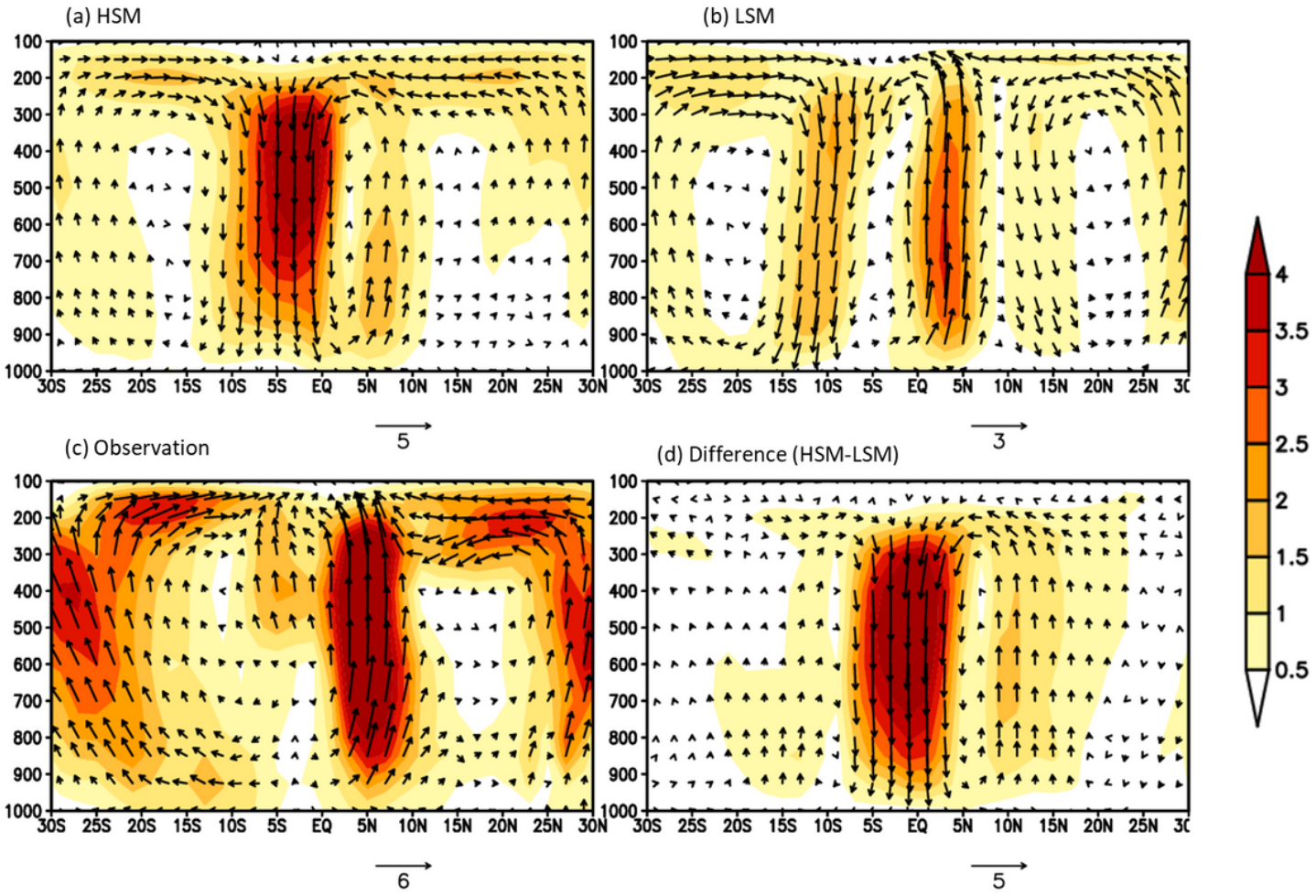

Figure 10

Regression maps of DMI (OND) onto NEM Hadley circulation for a period 1979-2005 for (a) HSM (b) LSM (c) Observation and (d) HSM-LSM difference

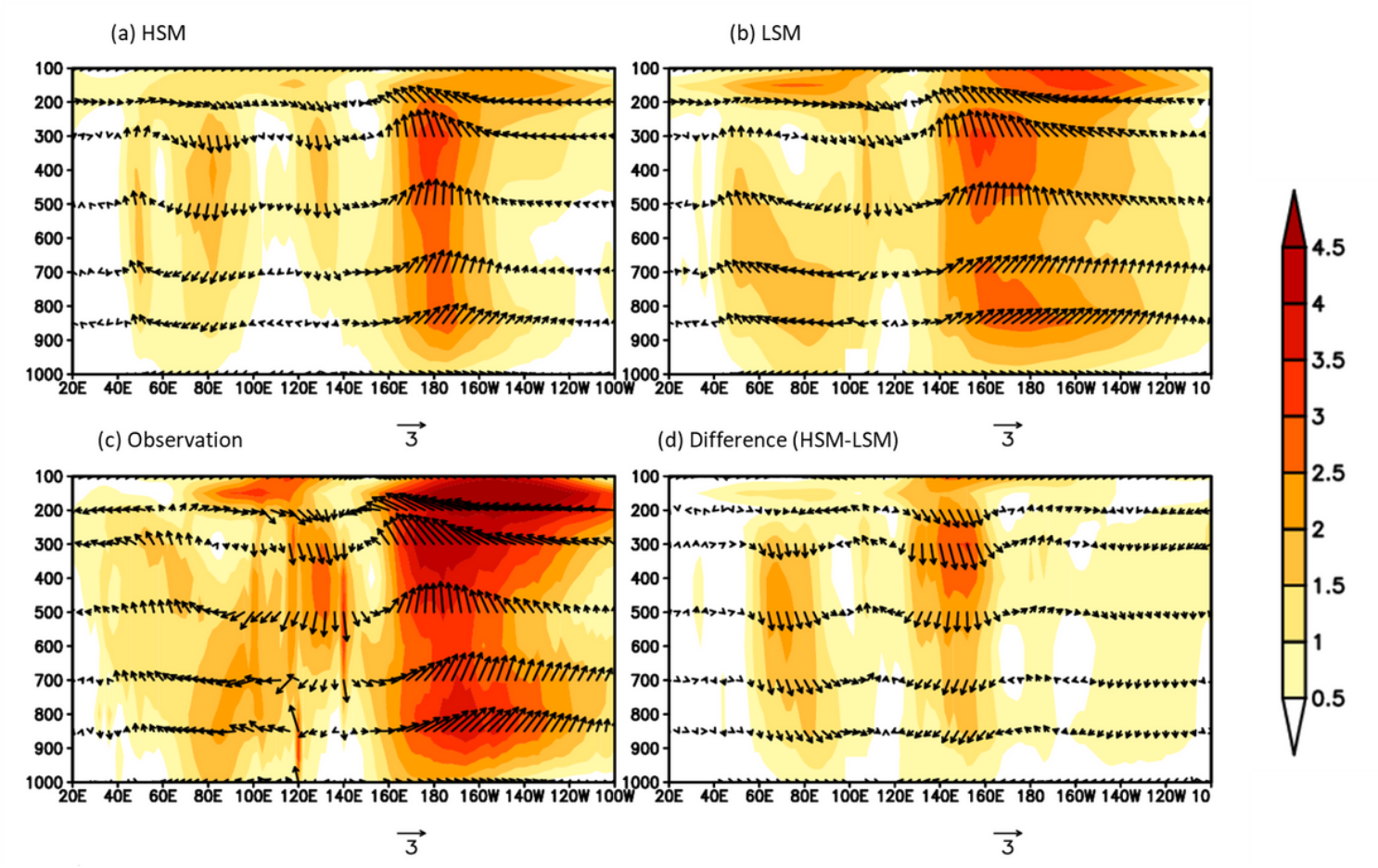

Figure 11

Regression maps of Nino 3.4 SST (OND) onto NEM Walker (5°S-5°N) circulation for a period 1979-2005 for (a) HSM (b) LSM (c) Observation and (d) HSM-LSM difference

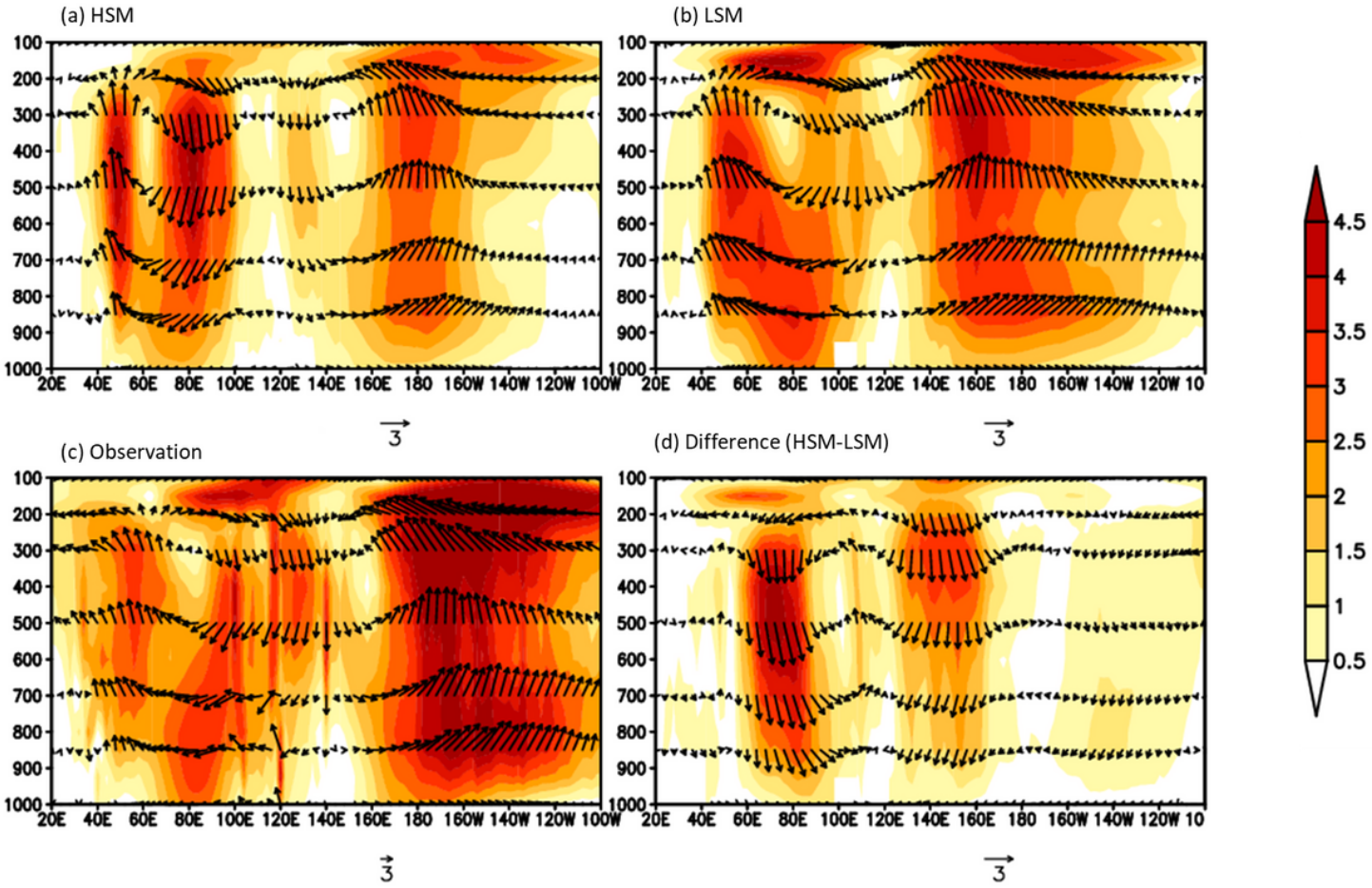

Figure 12

Regression maps of DMI (OND) onto NEM Walker (5°S-5°N) circulation for a period 1979-2005 for (a) HSM (b) LSM (c) Observation and (d) HSM-LSM difference

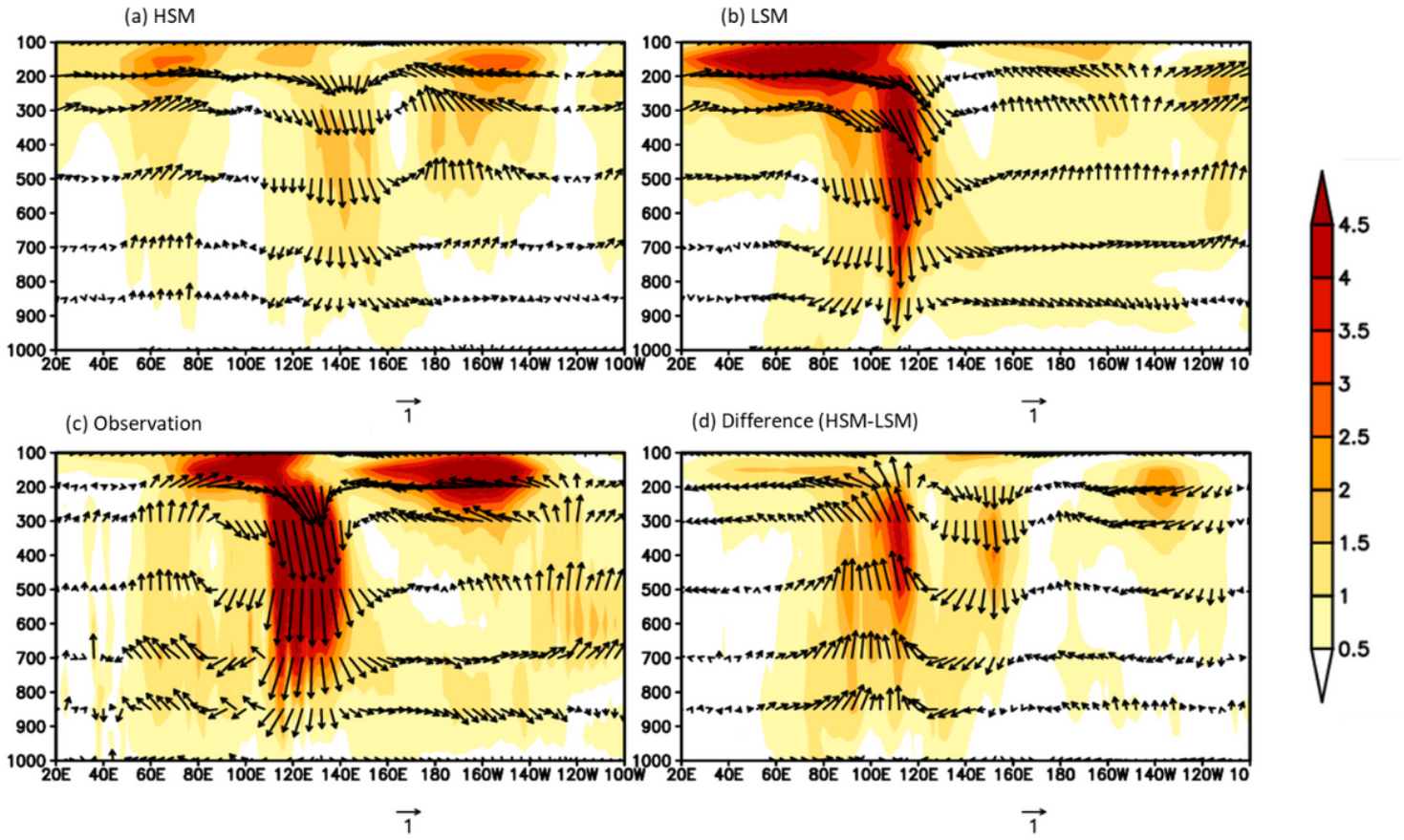

Figure 13

Regression maps of Nino 3.4 SST (OND) onto NEM Walker (5°N-15°N) circulation for a period 1979-2005 for (a) HSM(b) LSM (c) Observation and (d) HSM-LSM difference

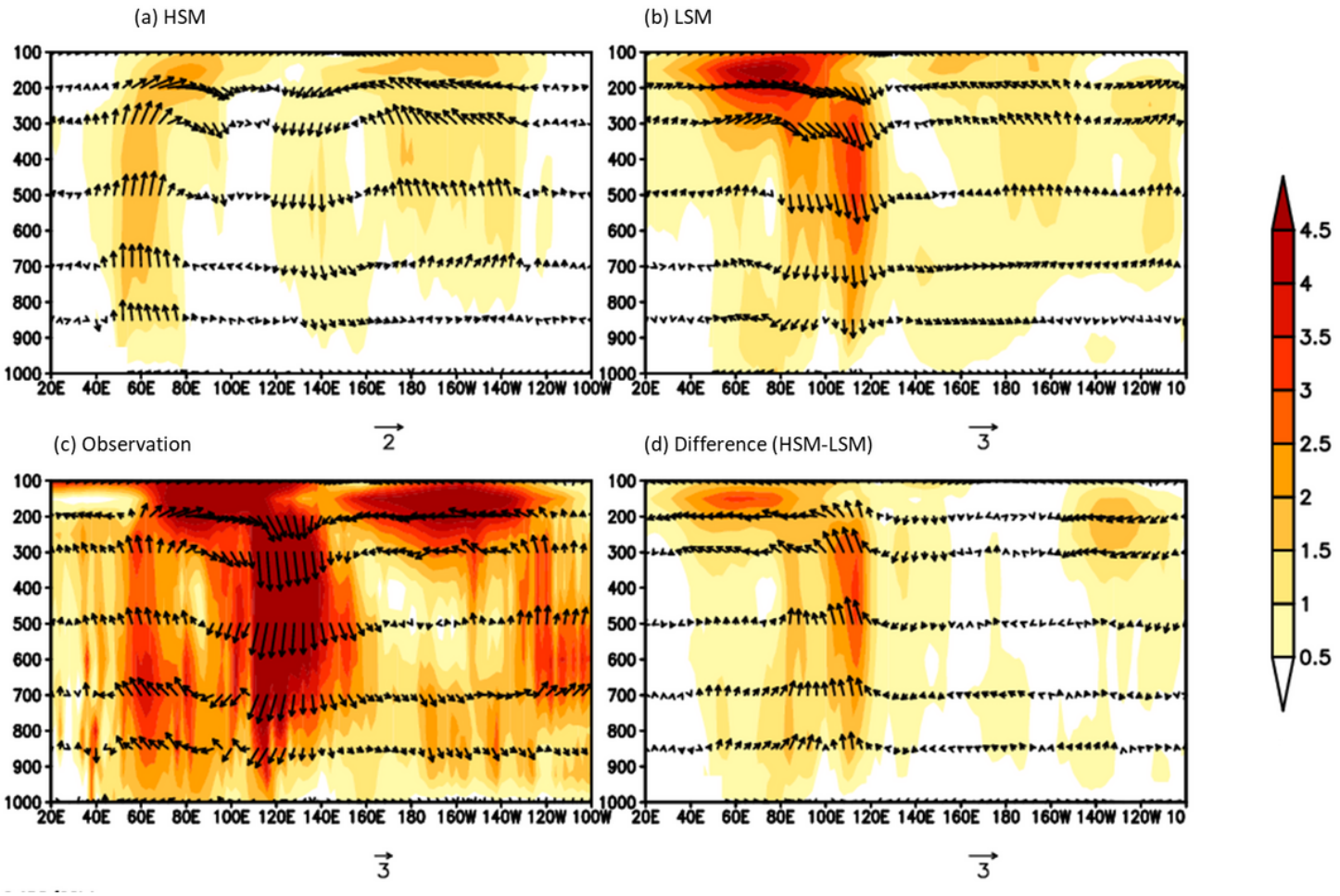

Figure 14

Regression maps of DMI(OND) onto NEM Walker (5°N-15°N) circulation for a period 1979-2005 for (a) HSM(b) LSM (c) Observation and (d) HSM-LSM difference